

Proposal for J-PARC 50 GeV Proton Synchrotron

## Gamma-ray spectroscopy of light hypernuclei

Y. Fujii, K. Futatsukawa, O. Hashimoto, K. Hosomi, H. Kanda, M. Kaneta, T. Koike, Y. Ma,  
K. Maeda, A. Matsumura, M. Mimori, S.N. Nakamura, K. Nonaka, Y. Okayasu, T. Suzuki,  
K. Shirotori, H. Tamura(spokesperson), K. Tsukada, M. Ukai

*Tohoku University, Japan*

K. Aoki, Y. Kakiguchi, T. Nagae, H. Noumi, Y. Sato, M. Sekimoto, H. Takahashi,  
T. Takahashi, A. Toyoda

*High Energy Accelerator Research Organization (KEK), Japan*

P. Evtoukhovitch, V. Kalinnikov, W. Kallies, N. Kravchuk, A. Moiseenko, D. Mzhavia,  
V. Samoilov, Z. Tsamalaidze, O. Zaimidoroga

*Joint Institute for Nuclear Research, Russia*

Y.Y. Fu, C.B. Li, X.M. Li, J. Zhou, S.H. Zhou, L.H. Zhu

*China Institute of Atomic Energy, China*

E. V. Hungerford, A. Lan (+ a postdoc and 2 graduate students)

*University of Houston, U.S.A.*

T. Bressani, S. Bufalino, L. Busso, D. Faso, A. Feliciello, S. Marcello,

*University of Torino and INFN, Sezione di Torino, Italy*

S. Kamigaito, K. Imai, K. Miwa, K. Tanida

*Kyoto University, Japan*

H. Fujioka, D. Nakajima, T.N. Takahashi

*University of Tokyo, Japan*

P. Markowitz, J. Reinhold

*Florida International University, U.S.A.*

K. Nakazawa, T. Watanabe

*Gifu University, Japan*

S. Minami, T.R. Saito

*GSI, Germany*

A. Krutenkova, V. Kulikov

*Institute for Theoretical and Experimental Physics, Russia*

R. E. Chrien  
*Brookhaven National Laboratory, U.S.A.*

O. Morra  
*INAF-IFSI and INFN, Sezione di Torino, Italy*

P.K. Saha  
*Japan Atomic Energy Agency, Japan*

T. Fukuda  
*Osaka Electro-Communication University, Japan*

S. Ajimura  
*Osaka University, Japan*

J.K. Ahn  
*Pusan University, Korea*

H.C. Bhang  
*Seoul National University, Korea*

M. Agnello  
*Torino Polytechnic and INFN, Italy*

## abstract

We propose to study structure of several light hypernuclei ( ${}^4_{\Lambda}\text{He}$ ,  ${}^7_{\Lambda}\text{Li}$ ,  ${}^{10}_{\Lambda}\text{B}$ ,  ${}^{11}_{\Lambda}\text{B}$ , and  ${}^{19}_{\Lambda}\text{F}$ ) by high-precision  $\gamma$  spectroscopy technique. Employing the K1.8 beam line and the SKS spectrometer system, we produce excited states of these hypernuclei using 1.5 GeV/ $c$  ( $K^-$ ,  $\pi^-$ ) reaction. We detect  $\gamma$  rays from hypernuclei using Hyperball-J, a newly-constructed large germanium detector array dedicated to hypernuclear  $\gamma$ -ray spectroscopy at J-PARC. We request 300 hours for tuning and 1000 hours for data-taking with  $0.5 \times 10^6$   $K^-$  beam per spill.

(1) One of the purposes of the experiment is to measure the reduced transition probabilities ( $B(M1)$ ) of the  $\Lambda$  spin-flip M1 transitions and extract the g-factor of a  $\Lambda$  inside a nucleus. We measure the  $M1(3/2^+ \rightarrow 1/2^+)$  transition of  ${}^7_{\Lambda}\text{Li}$ , where the  $3/2^+$  state is populated from the  $1/2^+(T=1)$  state via the fast  $1/2^+(T=1) \rightarrow 3/2^+$  transition.  $\text{Li}_2\text{O}$  target is used to optimize the stopping time in the target for Doppler shift attenuation method.

(2) Another purpose is to investigate the  $\Lambda N$  interaction further than our previous studies.

(2-1) In order to solve the present puzzles and establish the strengths of the  $\Lambda N$  spin-dependent (spin-spin, spin-orbit, and tensor) interactions, as well as to understand the  $\Sigma N$ - $\Lambda N$  coupling force, we take complete data for  ${}^{10}_{\Lambda}\text{B}$  and  ${}^{11}_{\Lambda}\text{B}$  in which the puzzles have arisen. For  ${}^{10}_{\Lambda}\text{B}$ , the ground state doublet ( $2^-, 1^-$ ) spacing will be determined unless the spacing is very small ( $|E(2^-) - E(1^-)| < 50$  keV), by using both spin-flip and non-spin-flip populations. As for  ${}^{11}_{\Lambda}\text{B}$ , we will observe ten or more transitions and construct the levels scheme of  ${}^{11}_{\Lambda}\text{B}$  using  $\gamma\gamma$  coincidence measurement.

(2-2) We will also run for a  ${}^{19}\text{F}$  target and detect both  ${}^{19}_{\Lambda}\text{F}(1/2^- \rightarrow 3/2^+, 1/2^+)$  transitions to determine the ground state doublet spacing. It gives the strength of the effective  $\Lambda N$  spin-spin interaction in the  $sd$ -shell hypernuclei for the first time and provides information on the radial dependence of the interaction.

(2-3) We also plan to run with a  ${}^4\text{He}$  (liquid helium) target and determine the ground state doublet ( $1^+, 0^+$ ) spacing precisely, in order to clarify the long-standing puzzle of an extremely-large charge symmetry breaking in the  $\Lambda N$  interaction. The cross sections of the spin-flip  ${}^4\text{He}(1^+)$  and non-spin-flip  ${}^4\text{He}(0^+)$  states will be also measured for several  $K^-$  momenta to confirm the spin-flip/non-spin-flip property of hypernuclear production in the ( $K^-$ ,  $\pi^-$ ) reaction.

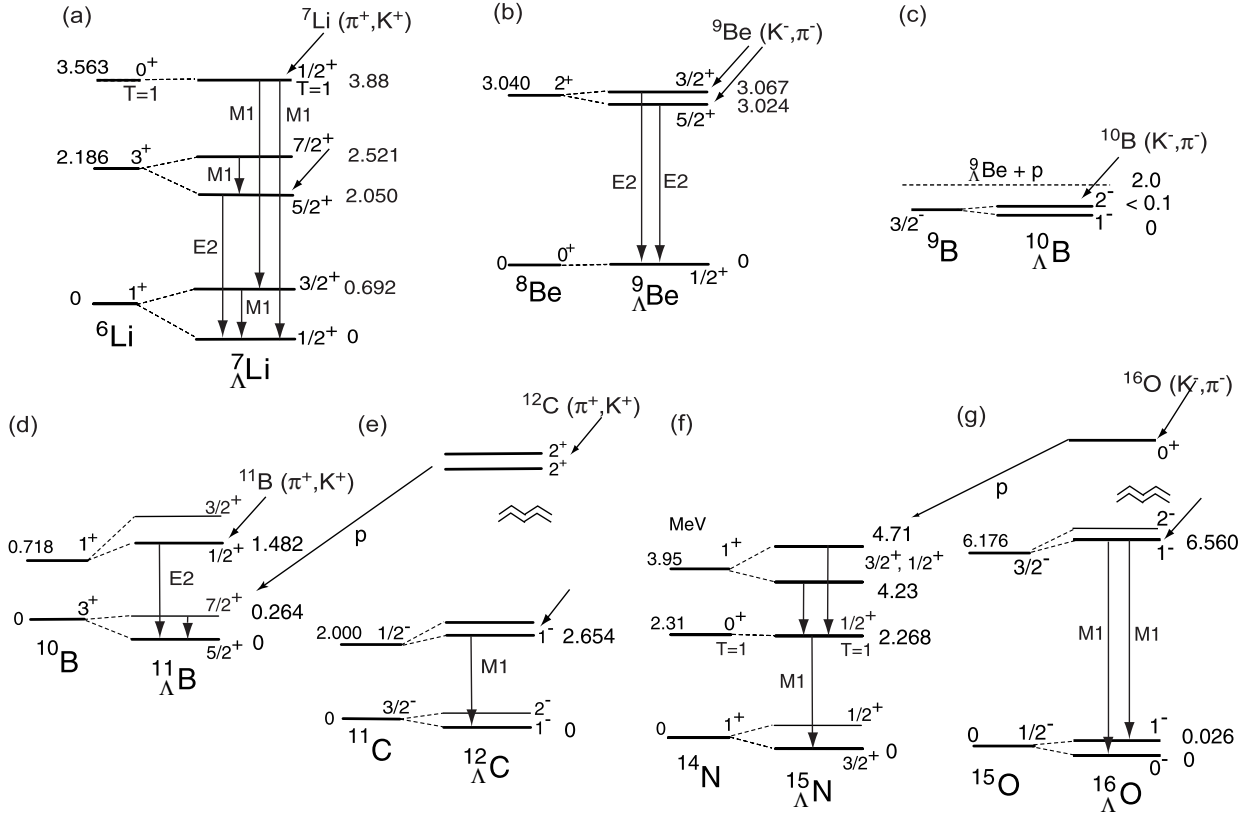


Figure 1: Level schemes of  ${}^7_{\Lambda}\text{Li}$ ,  ${}^9_{\Lambda}\text{Be}$ ,  ${}^{10}_{\Lambda}\text{B}$ ,  ${}^{11}_{\Lambda}\text{B}$ ,  ${}^{12}_{\Lambda}\text{C}$ ,  ${}^{15}_{\Lambda}\text{N}$  and  ${}^{16}_{\Lambda}\text{O}$  determined from our recent  $\gamma$ -ray spectroscopy experiments with Hyperball [1, 2, 3, 4, 5, 6, 7]. Observed  $\gamma$  transitions and measured level energies are indicated. Level schemes of corresponding core nuclei are also shown.

# 1 Introduction

## 1.1 Historical background

Precision  $\gamma$  spectroscopy using germanium (Ge) detectors, which is one of the most powerful means to study nuclear structure, has recently been introduced to hypernuclear physics. In 1998 we constructed Hyperball, a large-acceptance Ge detector array equipped with fast readout electronics, and succeeded in observing hypernuclear  $\gamma$  rays for the first time with Ge detectors under severe backgrounds from high energy meson beams [1, 2]. The energy resolution of hypernuclear levels, which was typically a few MeV (FWHM) by magnetic spectrometers, has been drastically improved to a few keV (FWHM) by Ge detectors. Since then we have observed many  $\gamma$  transitions from several  $p$ -shell  $\Lambda$  hypernuclei,  ${}^7_{\Lambda}\text{Li}$ ,  ${}^9_{\Lambda}\text{Be}$ ,  ${}^{11}_{\Lambda}\text{B}$ ,  ${}^{12}_{\Lambda}\text{C}$ ,  ${}^{15}_{\Lambda}\text{N}$  and  ${}^{16}_{\Lambda}\text{O}$ , in KEK E419, E509, E518, E566 and BNL E930 experiments [1, 2, 3, 4, 5, 6, 7], as shown in Fig. 1. Precision hypernuclear  $\gamma$  spectroscopy is now recognized as a new frontier in strangeness nuclear physics.

The study of hyperon-nucleon ( $YN$ ) and hyperon-hyperon ( $YY$ ) interactions is one of the

most important subjects in strangeness nuclear physics. Precise data of detailed level structure of various light  $\Lambda$  hypernuclei have provided us with quantitative information on the  $\Lambda N$  interaction as described in Sect. 2.1.1. Our study of  $\Lambda N$  interaction is the first step toward unified understanding of the baryon-baryon interactions and high density nuclear matter in which strangeness is expected to play an essential role.

In addition, using the precision  $\gamma$  spectroscopy technique, the hypernuclear shrinking effect was experimentally confirmed by measuring the  $E2$  transition probability  $B(E2)$  for the first time [2]. Thus, “impurity nuclear physics” can be explored, in which drastic changes of nuclear structure induced by a hyperon will become visible by hypernuclear  $\gamma$  spectroscopy.

Another physics possibility is to study possible modification of baryons in nuclear matter using a  $\Lambda$  in a hypernucleus. As described in Sect. 2.1.1, the magnetic moment of a  $\Lambda$  in a nucleus can be measured from  $B(M1)$  values by  $\gamma$  spectroscopy.

## 1.2 Strategy of the hypernuclear $\gamma$ spectroscopy at J-PARC

In the Letter Of Intent (LOI) titled “New Generation Spectroscopy of Hadron Many-Body Systems with Strangeness  $S = -2$  and  $-1$ ” [8], we proposed  $\gamma$ -ray spectroscopy of  $\Lambda$  hypernuclei together with spectroscopic studies of  $\Xi$  and  $\Lambda\Lambda$  hypernuclear systems. This LOI was classified as one of the Day-1 experiments by the Nuclear and Particle Physics Facility Committee.

As described in the LOI, our  $\gamma$  spectroscopy project at the J-PARC 50 GeV PS aims at systematic investigation of various bound-state levels of many  $\Lambda$  hypernuclei ranging from  ${}^4_{\Lambda}\text{He}$  to  ${}^{208}_{\Lambda}\text{Pb}$ , by taking advantage of high-intensity  $K^-$  beams, mainly with the  $(K^-, \pi^-)$  reaction and then also with the  $(K^-, \pi^0)$  reaction.

Here we will use a new-generation Ge detector array, “Hyperball-J”, with a higher efficiency and more tolerance to higher background rate for J-PARC experiments. Hyperball-J is under construction with the Grant-In-Aid for Priority Areas “Quark many-body systems with strangeness” (2005-2009).

The whole project, which consists of many experiments, takes several years or more and some of the experiments require full beam intensity after the LINAC and PS energy recovery (50 GeV,  $15\mu\text{A}$ ). Here, as a Day-1 experiment at the J-PARC, we propose the first experiment assuming the 30 GeV,  $9\mu\text{A}$  proton beam. We investigate several light  $\Lambda$  hypernuclei,  ${}^4_{\Lambda}\text{He}$ ,  ${}^7_{\Lambda}\text{Li}$ ,  ${}^{10}_{\Lambda}\text{B}$ ,  ${}^{11}_{\Lambda}\text{B}$ , and  ${}^{19}_{\Lambda}\text{F}$  using the  $(K^-, \pi^-)$  reaction at the K1.8 (or K1.1) beam line and employing the SKS spectrometer and Hyperball-J.

## 2 Motivation and experimental method

The purposes of the experiment are (1) the first precise measurement of the  $\Lambda$ -spin-flip  $B(M1)$  to investigate the magnetic moment of a  $\Lambda$  in a nucleus, and (2) further study of  $\Lambda N$  interaction to establish the spin-dependent  $\Lambda N$  interaction strengths and to clarify the  $\Lambda N$ - $\Sigma N$  coupling force as well as the charge symmetry breaking effect in  $\Lambda N$  interaction.

## 2.1 $B(M1)$ measurement and medium effect of baryons

### 2.1.1 Motivation

Using hyperons free from Pauli effect, we can investigate possible modification of baryons in nuclear matter through magnetic moments of hyperons in a nucleus.

The magnetic moments of baryons can be well described by the picture of constituent quark models in which each constituent quark has a magnetic moment of a Dirac particle having a constituent quark mass. If the mass (or the size) of a baryon is changed in a nucleus by possible partial restoration of chiral symmetry, the magnetic moment of the baryon may be changed in a nucleus. A  $\Lambda$  particle in a hypernucleus is the best probe to see whether such an effect really exists or not.

Possible change of the magnetic moment of a  $\Lambda$  in a nucleus has attracted attention of nuclear physicist. It was first pointed out [9] that Pauli effect in the quark level, if it exists, may modify a hyperon in a hypernucleus and change its magnetic moment. Then a calculation with the quark cluster model [10] showed that the ‘‘quark exchange current’’ between two baryons at a short distance changes the magnetic moment, of which effect depends on the confinement size of the hyperon in the nucleus.

Direct measurement of hypernuclear magnetic moments is extremely difficult because of its short lifetime for spin precession. An approach using heavy ion beams has been discussed [11] and recently proposed at GSI [12]. Here we propose to derive a  $g$ -factor of  $\Lambda$  in the nucleus from a probability ( $B(M1)$  value) of a spin-flip  $M1$  transition between the upper and lower members of a hypernuclear spin doublet. As shown in Fig. 2, each nuclear level in an ordinary nucleus (‘‘core’’ nucleus of hypernucleus) with non-zero spin splits into a doublet when a  $\Lambda$  hyperon is added. In the two states of this doublet, the  $\Lambda$  spin direction is opposite to each other with respect to the core spin, and the transition between the two members of the doublet corresponds to a flip of the  $\Lambda$  spin. In the weak coupling limit between the  $\Lambda$  and the core nucleus, the  $B(M1)$  of such a transition can be expressed as [13]

$$\begin{aligned}
 B(M1) &= (2J_{up} + 1)^{-1} | \langle \phi_{low} \| \boldsymbol{\mu} \| \phi_{up} \rangle |^2 \\
 &= (2J_{up} + 1)^{-1} | \langle \phi_{low} \| g_c \mathbf{J}_c + g_\Lambda \mathbf{J}_\Lambda \| \phi_{up} \rangle |^2 \\
 &= (2J_{up} + 1)^{-1} | \langle \phi_{low} \| g_c \mathbf{J} + (g_\Lambda - g_c) \mathbf{J}_\Lambda \| \phi_{up} \rangle |^2 \\
 &= \frac{3}{8\pi} \frac{(2J_{low} + 1)}{(2J_c + 1)} (g_c - g_\Lambda)^2
 \end{aligned} \tag{1}$$

here  $g_c$  and  $g_\Lambda$  denote effective  $g$ -factors of the core nucleus and the  $\Lambda$  hyperon,  $\mathbf{J}_c$  and  $\mathbf{J}_\Lambda$  denote their spins, and  $\mathbf{J} = \mathbf{J}_c + \mathbf{J}_\Lambda$  is the spin of the hypernucleus, respectively. Here the spatial components of the wave functions for the lower state and the upper state of the doublet,  $\phi_{low}$  and  $\phi_{up}$  (with spin  $J_{low}$  and  $J_{up}$ ) can be assumed to be identical.

In this study, effect of the meson exchange current between a  $\Lambda$  and a nucleon has to be considered. The meson exchange current is expected to be totally different from the  $NN$  case, because in the  $\Lambda N$  interaction one-pion exchange is forbidden but  $\Lambda N$ - $\Sigma N$  coupling makes another effect. The  $B(M1)$  values and the magnetic moments of several  $s$ ,  $p$ -shell hypernuclei were calculated in order to investigate such effects [14]. These effects were found to be of the

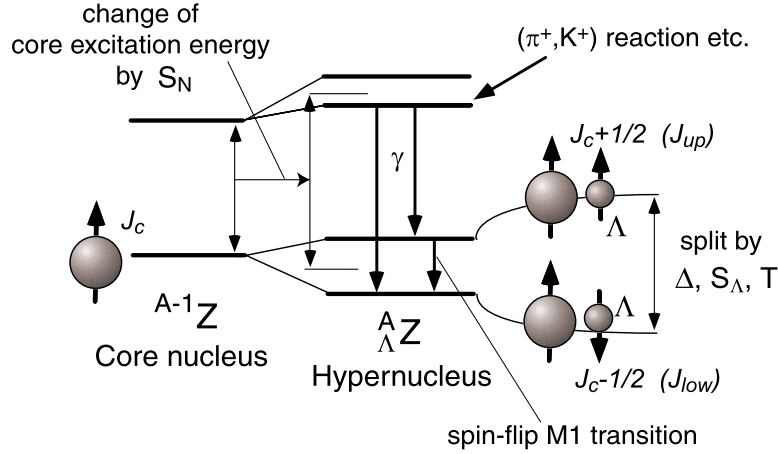


Figure 2: Spin doublet and spin-flip  $M1$  transition in a hypernucleus. When a  $\Lambda$  is coupled to the core nucleus with spin  $J_c$ , the level is split into a doublet ( $J_c + 1/2, J_c - 1/2$ ). The spin flip of the  $\Lambda$  gives rise to the  $M1$  transition from the upper to the lower state in the doublet, and its probability  $B(M1)$  is proportional to  $(g_c - g_\Lambda)^2$ , where  $g_c$  and  $g_\Lambda$  denote  $g$ -factors of the core nucleus and a  $\Lambda$  particle inside a nucleus (see text).

order of several %. For example,  $B(M1)$  of  ${}^7_\Lambda\text{Li}(3/2^+ \rightarrow 1/2^+)$  was calculated to be reduced by 7%. Accurate measurement of  $B(M1)$  values for several hypernuclei will also reveal the effect of the meson exchange current.

The reduced transition probability  $B(M1)$  can be derived from the lifetime  $\tau$  of the excited state as

$$1/\tau = \frac{16\pi}{9} E_\gamma^3 B(M1),$$

in which the lifetime is obtained by analyzing a partly-Doppler-broadened  $\gamma$ -ray peak shape when the stopping time of the recoiling excited hypernucleus in the target material is of the same order as the lifetime of the  $\gamma$ -emitting excited state. This method called Doppler shift attenuation method (DSAM) was once successfully applied to hypernuclei; as shown in the right inset of Fig. 6 (a), we measured the lifetime of the  ${}^7_\Lambda\text{Li}(5/2^+)$  state from the partly-Doppler-broadened peak shape of the  $5/2^+ \rightarrow 1/2^+$   $\gamma$  ray, and obtained the  $B(E2)$  value of this transition. The result confirmed the hypernuclear shrinking effect [2].

From this  ${}^7_\Lambda\text{Li}$  spectrum the  $B(M1)$  of the spin-flip  $3/2^+ \rightarrow 1/2^+$  transition was not able to be obtained, because the stopping time was too slow compared with the  $3/2^+$ -state lifetime and the  $\gamma$ -ray peak was fully broadened by Doppler shift. After that, the measurement of the  $\Lambda$ -spin-flip  $B(M1)$  has been attempted three times in BNL E930('01), KEK E581 and KEK E566, but accurate  $B(M1)$  measurement has not been achieved yet. In the E930('01) experiment, the spin-flip state of  ${}^7_\Lambda\text{Li}(3/2^+)$  was produced as a hyperfragment from highly excited unbound states of  ${}^{10}_\Lambda\text{B}$  by the reaction,  ${}^{10}\text{B}(K^-, \pi^-){}^{10}_\Lambda\text{B}^*, {}^{10}_\Lambda\text{B}^* \rightarrow {}^7_\Lambda\text{Li} + {}^3\text{He}$ . As shown in Fig. 3, the peak shape of the  ${}^7_\Lambda\text{Li}(3/2^+ \rightarrow 1/2^+, 692 \text{ keV})$  transition was analyzed and the lifetime of the  $3/2^+$  state was derived to be  $0.58^{+0.38}_{-0.20}$  ps (statistical error only), from which the  $B(M1)$  was obtained as  $0.30^{+0.12}_{-0.16} [\mu_N^2]$  (preliminary). This value corresponds to  $g_\Lambda = 1.1^{+0.4}_{-0.6} [\mu_N]$ , which

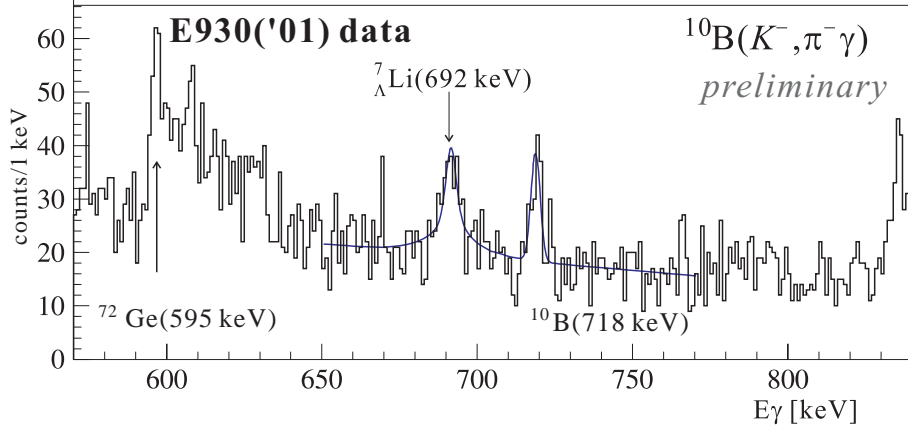


Figure 3: The  $\gamma$ -ray spectrum for the unbound region of  $^{10}_{\Lambda}\text{B}$  ( $-B_{\Lambda} = 0 - 40$  MeV) in the  $^{10}\text{B}(K^{-},\pi^{-})^{10}_{\Lambda}\text{B}$  reaction. The  $\gamma$ -ray peak for the  $^{7}_{\Lambda}\text{Li}(3/2^{+} \rightarrow 1/2^{+})$  was observed, where the  $^{7}_{\Lambda}\text{Li}(3/2^{+})$  state is mainly produced by  $^{10}_{\Lambda}\text{B}(s_n^{-1}s_{\Lambda}) \rightarrow ^{7}_{\Lambda}\text{Li} + ^3\text{He}$ . The peak shape is fitted well with a simulated peak for the  $^{7}_{\Lambda}\text{Li}(3/2^{+})$  lifetime of  $0.58^{+0.38}_{-0.20}$  ps (statistical only).

is compared with the free-space value of  $g_{\Lambda} = 1.226[\mu_N]$ . In order to measure the spin-flip  $B(M1)$  with better accuracy, we performed KEK E518 and E566. In E518, we observed six  $\gamma$  rays in  $^{11}_{\Lambda}\text{B}$  [6] but the complete level assignment was not possible because of low statistics which did not allow  $\gamma\gamma$  coincidence method. In E566, we observed the spin-flip  $M1$  transition of  $^{11}_{\Lambda}\text{B}(7/2^{+} \rightarrow 5/2^{+})$ , but unfortunately this transition energy is found to be much lower than expected and therefore the transition is too slow to measure the  $B(M1)$  by DSAM.

### 2.1.2 Experimental method

**Reaction** In the proposed experiment, we use the  $^{7}_{\Lambda}\text{Li}$  hypernucleus, because the bound-state level scheme of  $^{7}_{\Lambda}\text{Li}$  is perfectly known and the feasibility of the  $^{7}_{\Lambda}\text{Li} B(M1)$  measurement can be most unambiguously estimated. Figure 4 shows the level scheme of  $^{7}_{\Lambda}\text{Li}$ , where the excitation energies measured by our previous experiments are given. The calculated cross sections of the  $^{7}_{\Lambda}\text{Li}$  bound states by 1.5 GeV/c ( $K^{-},\pi^{-}$ ) reaction are shown in Fig. 5. When the  $^{7}_{\Lambda}\text{Li}$  is produced by the  $^{7}\text{Li}(K^{-},\pi^{-})^{7}_{\Lambda}\text{Li}$  reaction, the  $3/2^{+}$  state in the ground state doublet is produced by the spin-flip reaction, while the  $1/2^{+}$  state (ground state) is produced by the non-spin-flip reaction. We plan to measure the  $B(M1)$  of the spin-flip  $M1(3/2^{+} \rightarrow 1/2^{+})$  transition at 692 keV. The spin-flip  $3/2^{+}$  state is produced via the  $1/2^{+}(T=1)$  state at 3.88 MeV though the fast  $\gamma$  decay  $1/2^{+}(T=1) \rightarrow 3/2^{+}$ , as well as directly populated by the spin-flip ( $K^{-},\pi^{-}$ ) reaction at large angles ( $> 8^{\circ}$ ). The  $1/2^{+}(T=1)$  state is populated by non-spin-flip reaction with a large cross section. Therefore, the yield of the  $3/2^{+} \rightarrow 1/2^{+}$  is large, as experimentally known in our first Hyperball experiment [1].

In addition, we can directly populate the spin-flip  $7/2^{+}$  state at large scattering angles ( $> 8^{\circ}$ ). This state deexcites to the  $5/2^{+}$  and  $3/2^{+}$  states by emitting  $\gamma$  rays of 471 keV and 1829 keV (see Fig. 4). The peak shapes and branching ratios of these  $\gamma$  rays also provide a  $B(M1)$  value of the spin-flip  $7/2^{+} \rightarrow 5/2^{+}$  transition.

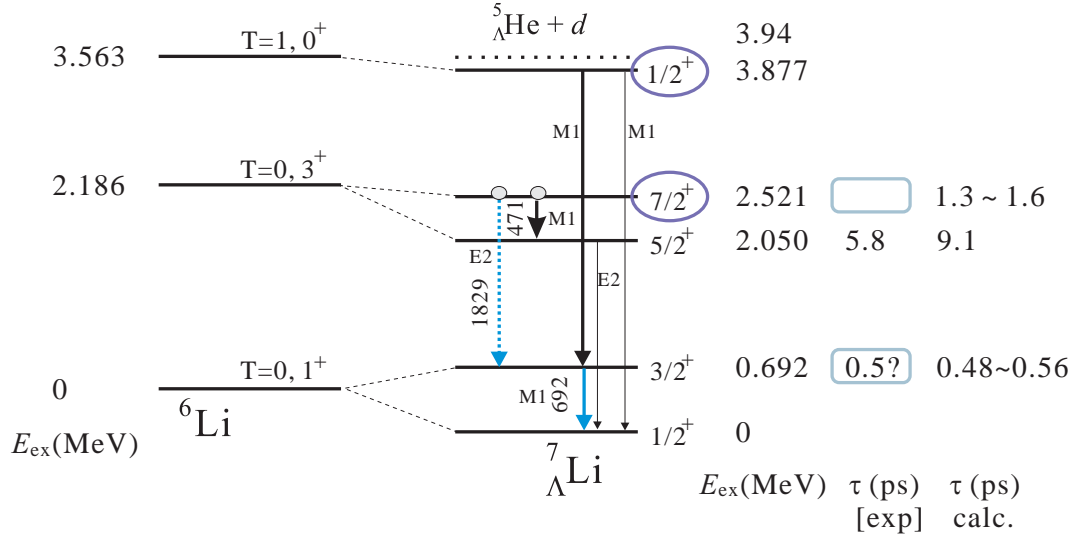


Figure 4: Level scheme of the  ${}^7_{\Lambda}\text{Li}$  hypernucleus. Excitation energies of all the bound states are experimentally determined [1, 7].

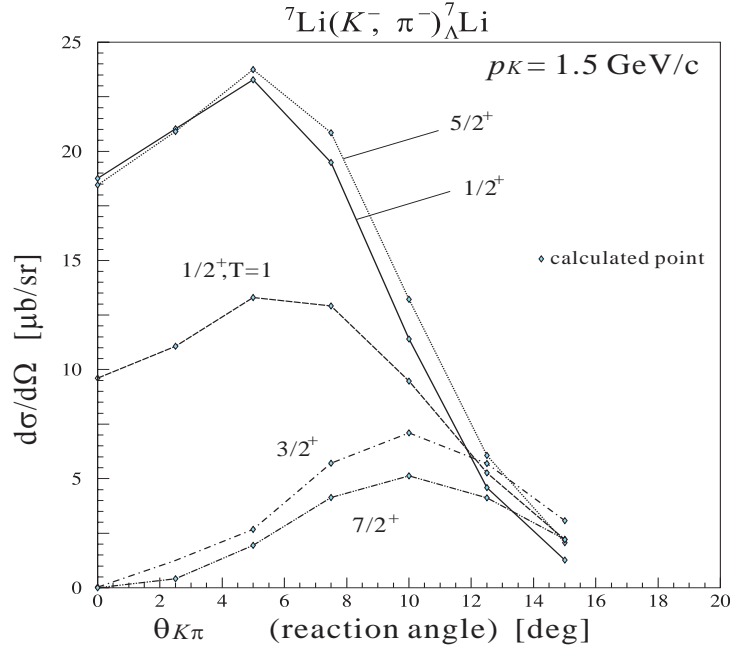


Figure 5: Cross sections of all the bound states of the  ${}^7_{\Lambda}\text{Li}$  hypernucleus in the  $(K^-, \pi^-)$  reaction at  $p_{K^-} = 1.5 \text{ GeV}/c$  calculated by Motoba [15].

**Lifetime and Target** Without any anomalous effect in  $g_{\Lambda}$ , the  $B(M1)$  value of this transition is estimated to be  $B(M1) = 0.326 [\mu_N^2]$  from Eq. 1 and calculated to be  $B(M1) = 0.322 [\mu_N^2]$  from a cluster model [16], which corresponds to 0.5 ps of the  $3/2^+$  state lifetime. In order to measure the lifetime by DSAM, we use a  $\text{Li}_2\text{O}$  target with a density of  $2.01 \text{ g}/\text{cm}^3$  in granular powder instead of lithium metal (density  $0.5 \text{ g}/\text{cm}^3$ ). The stopping time of the recoiling  ${}^7_{\Lambda}\text{Li}$

hypernuclei in this material is calculated to be 2–3 ps, while the expected lifetime of the  $3/2^+$  state is around 0.5 ps. According to our simulation for DSAM, the lifetime can be most accurately determined when the stopping time is 2–3 times longer than the lifetime. The present condition is close to this ideal condition. Although we produce the  $3/2^+$  state via the  $1/2^+(T=1) \rightarrow 3/2^+$  transition, this transition is fast (theoretically estimated to be 0.1 fs) and does not affect the lifetime measurement of the  $3/2^+$  state.

**Background** The  $^{16}\text{O}$  nuclei in the target make background. In the  $^7_\Lambda\text{Li}$  mass spectrum, bound states of  $^{16}_\Lambda\text{O}$  appear at the same mass region as the  $^7_\Lambda\text{Li}$  bound states and make significant backgrounds in the  $^7_\Lambda\text{Li}$   $\gamma$ -ray spectrum after selecting the  $^7_\Lambda\text{Li}$  bound-state region. Although the continuous background level is higher than the lithium target case, no  $\gamma$ -ray lines from  $^{16}\text{O}$  target appear around the  $^7_\Lambda\text{Li}(3/2^+ \rightarrow 1/2^+)$  energy (692 keV); there are only four bound states in  $^{16}_\Lambda\text{O}$  and all the  $\gamma$  transitions from them were measured at 6–7 MeV in E930 [4], and there are no  $\gamma$  rays from ordinary nuclei with the mass number less than 16.

Several neutron-induced  $\gamma$ -ray lines from ordinary nuclei in the surrounding material appear in the  $\gamma$ -ray spectrum. Among them, the 692 keV  $\gamma$  ray from  $^{72}\text{Ge}(n, n')$  can be a background for our measurement, although the lifetime of  $^{72}\text{Ge}(692)$   $\gamma$  ray is slow (641 ns) and a prompt timing cut (typically  $< 20$  ns) almost removes this  $\gamma$  ray. According to our experience in E419 (see Fig. 6 (b)), a small peak from  $^{72}\text{Ge}$  appears at 692 keV when the prompt timing cut is loose (75 ns gate width). This background is estimated to give almost negligible effect to the  $^7_\Lambda\text{Li}$   $\gamma$ -ray spectrum after the tight timing cut (15 ns gate width), and this effect can be reliably estimated from intensities of other lines such as  $^{74}\text{Ge}(596)$  and  $^{72}\text{Ge}(834)$ .

## 2.2 $\Lambda N$ interaction

From detailed level structure of several light hypernuclei, we can extract the strengths of the  $\Lambda N$  spin-dependent (spin-spin, spin-orbit, and tensor) interactions, and then investigate the  $\Sigma N$ - $\Lambda N$  coupling force and a possible charge symmetry breaking effect.

Experimental information on these characteristics of the  $\Lambda N$  interaction plays an essential role to discriminate and improve baryon-baryon interaction models, not only those based on meson-exchange picture but also those including quark-gluon degree of freedom, toward unified understanding of the baryon-baryon interactions. For example, the very small  $\Lambda$ -spin-dependent spin-orbit force established by our recent  $\gamma$  spectroscopy experiments of  $^9_\Lambda\text{Be}$  [3] and  $^{13}_\Lambda\text{C}$  [17] suggest that the quark-gluon picture is valid for the spin-orbit force rather than the meson-exchange picture [18], while the  $\Lambda N$  tensor force strength determined from our  $^{16}_\Lambda\text{O}$   $\gamma$  spectroscopy data [7] is explained well in the meson-exchange framework. In addition, understanding of the  $YN$  and  $YY$  interactions is essential to describe high density nuclear matter containing hyperons which may be realized in the center of neutron stars.

**Spin-dependent  $\Lambda N$  forces** The  $\Lambda N$  interaction can be expressed as

$$V_{\Lambda N}(r) = V_0(r) + V_\sigma(r)\mathbf{s}_N\mathbf{s}_\Lambda + V_\Lambda(r)\mathbf{l}_{N\Lambda}\mathbf{s}_\Lambda + V_N(r)\mathbf{l}_{N\Lambda}\mathbf{s}_N + V_T(r)[3(\boldsymbol{\sigma}_N\hat{\mathbf{r}})(\boldsymbol{\sigma}_\Lambda\hat{\mathbf{r}}) - \boldsymbol{\sigma}_N\boldsymbol{\sigma}_\Lambda] \quad (2)$$

In shell-model description of  $p$ -shell hypernuclei, the effective  $s_\Lambda p_N$  (and  $p_\Lambda s_N$ ) interactions have five radial integrals corresponding to each of the five terms in Eq. 2, denoted by  $\bar{V}$ ,  $\Delta$ ,  $S_\Lambda$ ,  $S_N$

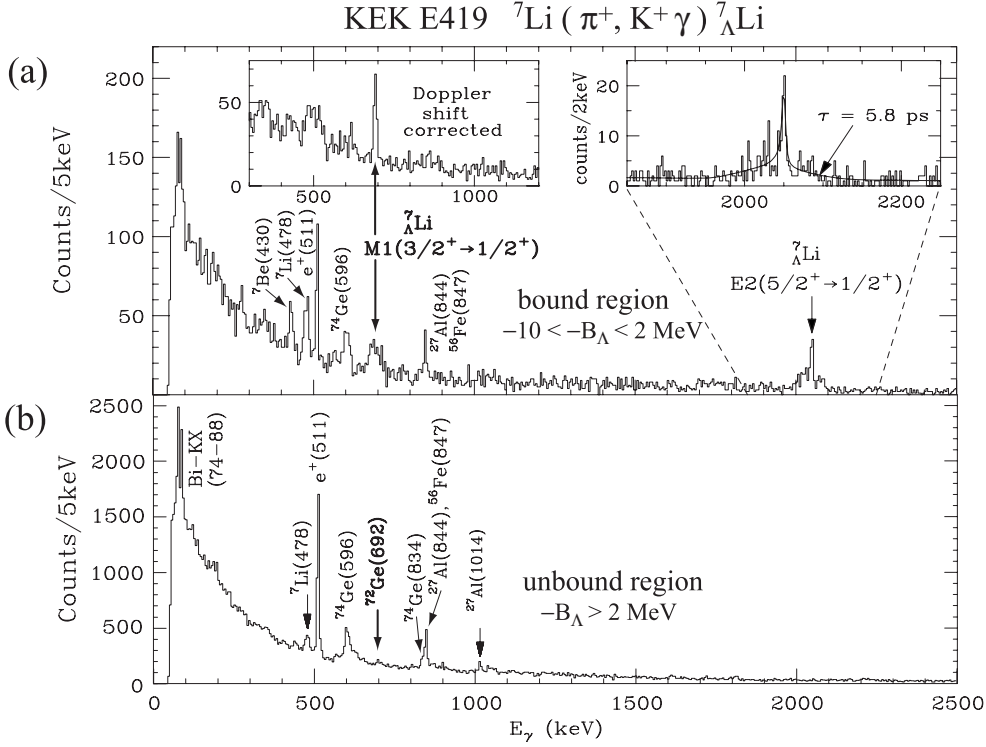


Figure 6:  $\gamma$ -ray spectrum of  ${}^7_{\Lambda}\text{Li}$  measured in KEK E419 [1]. (a) When the bound state region is selected,  ${}^7_{\Lambda}\text{Li}$   $\gamma$ -rays were observed. The broad peak at 692 keV, which becomes sharp after event-by-event Doppler-shift correction (see the upper left inset), is assigned to the spin-flip  $M1(3/2^+ \rightarrow 1/2^+)$  transition. The partly-broadened peak at 2050 keV is assigned to the  $E2(5/2^+ \rightarrow 1/2^+)$  transition. By comparing this peak with simulated peak shapes, the lifetime of the  $5/2^+$  state was obtained to be  $5.8_{-0.7}^{+0.9} \pm 0.7$  ps (see the upper right inset). (b) When the unbound region of  ${}^7_{\Lambda}\text{Li}$  is selected, background  $\gamma$  rays from normal nuclei, particularly from fast-neutron induced  $\gamma$  rays from surrounding materials, are observed. In this spectrum, the timing cut is looser (75 ns gate width) than our usual condition (15 ns) and thus the background peak from  ${}^{72}\text{Ge}$  (lifetime of 641 ns) still remains at 692 keV.

and  $T$ , respectively [13, 19]. These integrals can be determined phenomenologically from low-lying level structure of  $p$ -shell hypernuclei. Before we started the hypernuclear  $\gamma$  spectroscopy project with Hyperball, the spin-dependent interaction strengths ( $\Delta$ ,  $S_\Lambda$ ,  $S_N$  and  $T$ ) were not well known; the available hypernuclear data were not of sufficient quality and quantity to unambiguously extract them. The study of these  $\Lambda N$  spin-dependent interactions have started using Hyperball. In KEK E419 and BNL E930, we observed several  $\gamma$  transitions in  ${}^7_{\Lambda}\text{Li}$ ,  ${}^9_{\Lambda}\text{Be}$ , and  ${}^{16}_{\Lambda}\text{O}$ , and the parameters of  $\Delta$ ,  $S_\Lambda$ ,  $S_N$  and  $T$  were determined from  ${}^7_{\Lambda}\text{Li}(3/2^+, 1/2^+)$  [1],  ${}^9_{\Lambda}\text{Be}(3/2^+, 5/2^+)$  [3, 5],  ${}^7_{\Lambda}\text{Li}(5/2^+, 1/2^+)$  [1], and  ${}^{16}_{\Lambda}\text{O}(1^-, 0^-)$  [4] spacings, respectively, as <sup>1</sup>

$$\Delta = 0.43 \text{ MeV}, S_\Lambda = -0.01 \text{ MeV}, S_N = -0.43 \text{ MeV}, T = 0.03 \text{ MeV}. \quad (3)$$

<sup>1</sup>These parameter values are slightly dependent on the mass number. The values shown here are for  $A = 7$  and the effect of the  $\Sigma N$ - $\Lambda N$  coupling is considered assuming a theoretical interaction model.

These obtained parameter values were compared with predicted values from theoretical baryon-baryon interaction models based on meson exchange picture or quark-gluon picture, in order to test their validity and to improve the models.

Although we determined the parameters from specific hypernuclear levels, universality of these parameter values to other hypernuclear levels has been checked, for example, using the  ${}^7_{\Lambda}\text{Li}(7/2^+, 5/2^+)$  spacing [7]. However, some recent data on  ${}^{10}_{\Lambda}\text{B}$  and  ${}^{11}_{\Lambda}\text{B}$  suggest that these parameters cannot explain their level energies as described in Sect 2.3 and more experimental data are necessary to investigate the universality of the parameters as well as the validity of the theoretical framework. Here, one of the most relevant effect to be investigated is the  $\Lambda N$ - $\Sigma N$  coupling which is considered to play an important role in a nucleus as described below.

Another approach is the exact few-body calculation of light hypernuclei from theoretically proposed models of baryon-baryon interactions. Hiyama et al. have calculated the structure of  ${}^4_{\Lambda}\text{He}$ ,  ${}^7_{\Lambda}\text{Li}$ ,  ${}^9_{\Lambda}\text{Be}$ , etc. based on various versions of the one-boson exchange (Nijmegen) baryon-baryon interaction model [20]. Then, comparison of the calculated results with our experimental data has revealed problems in the existing baryon-baryon models and showed how to improve the interaction models. In this approach, particularly important are the data of light hypernuclei such as  ${}^4_{\Lambda}\text{He}$ ,  ${}^7_{\Lambda}\text{Li}$ ,  ${}^9_{\Lambda}\text{Be}$ ,  ${}^{10}_{\Lambda}\text{B}$ ,  ${}^{11}_{\Lambda}\text{B}$ , etc. to which few body calculation (with  $\alpha$ -cluster model) can be applied.

**$\Lambda N$ - $\Sigma N$  coupling and the three-body force** The  $\Lambda N$ - $\Sigma N$  coupling gives rise to a mixing of  $\Lambda$  hypernuclear and  $\Sigma$  hypernuclear states and significantly affects the structure of hypernucleus. This effect is particularly important to understand  $YN$  interaction in a high density matter.

The two-body  $\Lambda N$ - $\Sigma N$  interaction can be incorporated into two-body effective  $\Lambda N$  interaction, while the three-body  $\Lambda NN$  force due to  $\Lambda N$ - $\Sigma N$  coupling as shown in Fig. 7 cannot. Therefore, hypernuclear level energies might not be able to be understood by the five terms of the  $\Lambda N$  two-body effective interaction in Eq. 2.

The  $\Lambda NN$  three-body force is expected to play a significant role in a nucleus; this three-body force should be stronger than the  $3N$  force including the intermediate  $\Delta$  states, since the  $\Sigma$  particle in intermediate state is only 80 MeV heavier than the  $\Lambda$  particle compared to the 300 MeV difference in the case of nucleon and  $\Delta$ . In addition, since the  $\Lambda NN$  force is mediated by two-pion exchange while one-pion exchange between a  $\Lambda$  and a nucleon is forbidden by isospin conservation, relative importance of the  $\Lambda NN$  force to the  $\Lambda N$  force is expected to be large.

It was recently understood that the three-body force gives rise to a large effect to the binding energies of the  $1^+$  and  $0^+$  states of  $A = 4$  hypernuclei and solves the long-standing puzzle on the binding energies of  $s$ -shell hypernuclei ( $A = 3, 4, 5$ ) [21]. Then the energy levels of  $s$ -shell hypernuclei have been exactly calculated through variational method from existing baryon-baryon interaction models with the  $\Lambda N$ - $\Sigma N$  coupling explicitly taken into account [22, 23]. Thus it was found that some of the interaction models reproduce the  $s$ -shell hypernuclear data rather well. However, we need to investigate more data for  $p$ -shell hypernuclei in order to reveal the properties of the  $\Lambda N$ - $\Sigma N$  coupling and the three-body force. On the other hand, quantitative evaluation of the three-body force effect for each hypernuclear level is necessary to extract the strengths of the four spin-dependent interactions reliably.

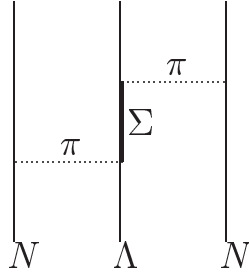


Figure 7: A diagram for the  $\Lambda NN$  three-body force due to intermediate  $\Sigma$  states introduced by  $\Lambda N$ - $\Sigma N$  couplings.

**Charge symmetry breaking** Another important subject in the study of  $\Lambda N$  interaction is the charge symmetry breaking (CSB) effect. Since a  $\Lambda$  has no isospin and no charge, the  $\Lambda p$  and  $\Lambda n$  interactions are the same if the charge symmetry holds exactly. However, as shown in Fig. 11 the  $\Lambda$  binding energies of the lightest mirror pair of hypernuclei,  ${}^4_{\Lambda}\text{H}$  and  ${}^4_{\Lambda}\text{He}$ , are known to have a large difference, and it is implied that the  $\Lambda p$  interaction is more attractive than the  $\Lambda n$  interaction. This effect can be precisely investigated from level structure of various mirror hypernuclei, rather than by  $YN$  scattering experiments where precise  $\Lambda n$  scattering experiments are almost impossible.

As for the origin of such large CSB effects, no conclusive remark is obtained yet, although several mechanisms such as  $\Lambda$ - $\Sigma^0$  mixing and  $\Lambda N$ - $\Sigma N$  coupling are proposed. In order to answer the question, to investigate the spin-dependence of the CSB interaction is very important. For example, the  $\Lambda$ - $\Sigma^0$  mixing model expects a CSB potential similar to that of one-pion exchange, which includes spin-spin and tensor forces, while it was suggested that the CSB potential is almost spin independent based on the  $A = 4$  hypernuclear data [24]. If the CSB potential is really spin independent,  $\Lambda$ - $\Sigma^0$  mixing is not a significant source of the CSB.

Another candidate for the origin of CSB is the  $\Lambda N$ - $\Sigma N$  coupling effect; CSB occurs through the mass difference of  $\Sigma^+$ ,  $\Sigma^0$ , and  $\Sigma^-$  which is some 8 MeV or about 10% of the  $\Sigma$ - $\Lambda$  mass difference. As described above, this mechanism also plays an essential role for the  $\Lambda NN$  three-body force. This fact implies that the CSB might appear in the  $\Lambda NN$  force as well as in the  $\Lambda N$  force.

Systematic study of various pairs of mirror hypernuclei to investigate the spin-dependence and possible three-body force components in CSB interaction is indispensable to clarify the characteristics and thus the origin of the CSB interaction.

## 2.3 Choice of the targets for YN interaction

### 2.3.1 ${}^{10}_{\Lambda}\text{B}$ and ${}^{11}_{\Lambda}\text{B}$

As described above, we have determined all the four parameters of the spin-dependent  $\Lambda N$  interaction strengths from  ${}^7_{\Lambda}\text{Li}$ ,  ${}^9_{\Lambda}\text{Be}$ , and  ${}^{16}_{\Lambda}\text{O}$  data, but our data on  ${}^{10}_{\Lambda}\text{B}$  and  ${}^{11}_{\Lambda}\text{B}$  cannot be consistently explained by these strengths. It has become clear that, in order to solve these puzzles and to establish the spin-dependent interaction strengths, the following studies are

necessary:

- Properties of the  $\Lambda N$ - $\Sigma N$  coupling force have to be investigated from various hypernuclear data. Then its effect to each hypernuclear level can be reliably estimated.
- When we derive information on the  $\Lambda N$  interaction from hypernuclear data, the wave functions of the core nuclei should be correctly known. Using plenty of level data of the hypernucleus, the wave function of the core nucleus can be improved.
- The nuclear size dependence of the parameters needs to be well studied from hypernuclear data with different mass numbers.

For these purposes, it is desirable to accumulate hypernuclear data for as many levels as possible over all the  $p$ -shell hypernuclei. In particular,  ${}^{10}_{\Lambda}\text{B}$ ,  ${}^{11}_{\Lambda}\text{B}$ ,  ${}^{12}_{\Lambda}\text{C}$  data are important, because the experimental data for these hypernuclear bound states are still limited and the existing data on  ${}^{10}_{\Lambda}\text{B}$  and  ${}^{11}_{\Lambda}\text{B}$  seem to be puzzling. The  ${}^{12}_{\Lambda}\text{C}$   $\gamma$ -ray data have recently been taken in the fall in 2005 at KEK (E566) and are under analysis now. So we propose to take high quality data for  ${}^{10}_{\Lambda}\text{B}$  and  ${}^{11}_{\Lambda}\text{B}$  in the proposed experiment. In addition, the few-body calculation approach, which is expected to treat well the three problems above, will be applied to these three hypernuclei by Hiyama via cluster model [25].

**${}^{10}_{\Lambda}\text{B}$**  The  $M1$  transition between the  ${}^{10}_{\Lambda}\text{B}$  ground-state doublet members ( $2^- \rightarrow 1^-$ ) was not observed in the previous experiments in spite of the expected large cross section of  $2^-$  [26, 5]. This result suggests the spacing of  $E(2^-) - E(1^-) < 100$  keV, where the  $\gamma$ -ray detection efficiency rapidly drops below 100 keV in these experiments. According to a shell model calculation [27], this spacing is expressed as

$$E(2^-) - E(1^-) = 0.579\Delta + 1.413S_{\Lambda} + 0.013S_N - 1.073T + \Lambda\Sigma, \quad (4)$$

where the  $\Lambda N$ - $\Sigma N$  coupling effect is estimated to be  $\Lambda\Sigma = -0.015$  MeV. The experimental result of  $E(2^-) - E(1^-) < 100$  keV is inconsistent with the parameter values in Eq. 3 giving  $E(2^-) - E(1^-) = 180$  keV; we need  $\Delta < 0.30$  MeV to explain the data.

Recently, Millener suggested that the value of  $\Delta$  may be much smaller ( $\Delta = 0.33$  MeV) for  ${}^{10}_{\Lambda}\text{B}$  and heavier hypernuclei due to a size effect. Considering possible variations of the core wave function, he predicts that the  ${}^{10}_{\Lambda}\text{B}$  spacing can be as small as 89 keV [28].

Since in the previous experiments the non-spin-flip reaction ( $0.8$ – $0.93$  GeV/ $c$  ( $K^-$ ,  $\pi^-$ ) reaction) was used, only the  $2^-$  state can be populated and the  $\gamma$  transition cannot be observed if the  $2^-$  state is the lower member of the doublet. In the proposed experiment, by using both spin-flip and non-spin-flip populations ( $1.5$  GeV/ $c$  ( $K^-$ ,  $\pi^-$ ) reaction) and irradiating much more  $K^-$  beams than the previous experiments, the ground state doublet spacing  ${}^{10}_{\Lambda}\text{B}(2^-, 1^-)$  can be determined for both cases of the spin ordering in the doublet unless the spacing is unfortunately very small ( $|E(2^-) - E(1^-)| < 50$  keV).

The weak decay of the upper member of the doublet may compete with the  $\gamma$  transition to the ground state. According to the expected  $B(M1)$  value, the transition rate<sup>2</sup> is  $(200 \text{ ps})^{-1}$

---

<sup>2</sup>The  $M1$  transition rate is proportional to  $E_{\gamma}^3$  where  $E_{\gamma}$  is the transition energy.

for 67 keV and  $(400 \text{ ps})^{-1}$  for 53 keV. Since the weak decay lifetime is around 200 ps [29], the  $\gamma$  transition is suppressed only by a factor of three for 53 keV.

In addition, we will be able to take a spectrum like Fig. 3 but with much higher statistics and obtain a byproduct result for  $B(M1)$  measurement of  ${}^7_{\Lambda}\text{Li}$ .

**${}^{11}_{\Lambda}\text{B}$**  The  ${}^{11}_{\Lambda}\text{B}$  hypernucleus is expected to have many bound states and is suitable for a test of the  $\Lambda N$  interaction parameters and the theoretical framework. In our previous experiment (KEK E518) by  $(\pi^+, K^+)$  reaction we observed six transitions of  ${}^{11}_{\Lambda}\text{B}$  (see Fig. 9) but most of them were not able to be assigned.

Figure 8 is the expected level scheme of  ${}^{11}_{\Lambda}\text{B}$ . The 1483 keV  $\gamma$ -ray peak was assigned to  $E2(1/2^+ \rightarrow 5/2^+(gs))$  transition [6]. But this energy is not explained by the interaction parameters; the result of Millener's shell-model calculation [27]:

$$E(1/2^+) - E(5/2^+) = -0.243\Delta - 1.234S_{\Lambda} - 1.090S_N - 1.627T + E_{core} \text{ (MeV)}, \quad E_{core} = 0.718$$

and the spin-dependent interaction parameter values determined from other hypernuclear data (Eq. 3) give 1020 keV. The 264 keV  $\gamma$  ray, which was also observed in the  ${}^{12}\text{C}(K^-, \pi^-)$  experiment (KEK E566), was assigned to the spin-flip M1 transition in the ground states doublet ( $7/2^+ \rightarrow 5/2^+$ ). This energy is also lower than the expected value of 418 keV and also suggesting a smaller value of  $\Delta \sim 0.33$  MeV. The other four  $\gamma$  rays were not able to be assigned.

To explain the level energies, we need to correctly estimate the  $\Lambda N$ - $\Sigma N$  coupling effect and/or to prepare a correct wave function for the core nucleus. More  ${}^{11}_{\Lambda}\text{B}$  data for level energies and their assignments are necessary to solve the problems.

In the proposed experiment, both spin-flip and non-spin-flip populations are available, and a higher efficiency of Hyperball-J and larger cross sections of  $(K^-, \pi^-)$  reaction allow  $\gamma\gamma$  coincidence measurement. They enable us to reconstruct the level scheme.

## 2.4 ${}^{19}_{\Lambda}\text{F}$

We will also run with a  ${}^{19}\text{F}$  target (using teflon  $(\text{CF}_2)_n$ ) to study  $sd$ -shell hypernuclei for the first time. Figure 10 is an expected level scheme and  $\gamma$  transition in  ${}^{19}_{\Lambda}\text{F}$ . Since the cross sections to populate the  $1/2^-(T=0)$  state with  $\Delta L = 1$  transition is expected to be large (of the order of  $40 \mu\text{b}/\text{sr}$  at  $2.5^0 - 10^0$ ), by the  $(K^-, \pi^-)$  reaction at 1.5 GeV/ $c$ , we can observe both  $E1(1/2^- \rightarrow 3/2^+, 1/2^+)$  transitions in  ${}^{19}_{\Lambda}\text{F}$  and determine the ground state doublet ( $3/2^+, 1/2^+$ ) spacing, which gives the strength of the effective  $\Lambda N$  spin-spin interaction in the  $sd$ -shell hypernuclei. The other excited states,  ${}^{19}_{\Lambda}\text{F}(1/2^+(T=1))$  and  ${}^{19}_{\Lambda}\text{F}(5/2^+)$ , are also expected to be populated with  $\Delta L = 0$  and 2 reactions, and the  $\gamma$  transitions of  $M1(1/2^+(T=1) \rightarrow 3/2^+, 1/2^+)$  and  $E2(1/2^+ \rightarrow 3/2^+, 1/2^+)$  are also expected, respectively, with less intensities. Since the  $1/2^+(T=1)$  and  $1/2^-; T=0$  states are populated by different  $\Delta L$  reactions, the transitions from these two states can be clearly discriminated with each other from angular distribution of the  $(K^-, \pi^-)$  reaction. The  $E2(1/2^+ \rightarrow 3/2^+, 1/2^+)$  transitions are also discriminated by their sharp peaks due to the slow transition rates.

The ground state doublet ( $3/2^+, 1/2^+$ ) spacing is roughly estimated to be 429 keV by Millener from the spin-spin interaction strength in the  $p$ -shell hypernuclei ( $\Delta = 0.43$  MeV).



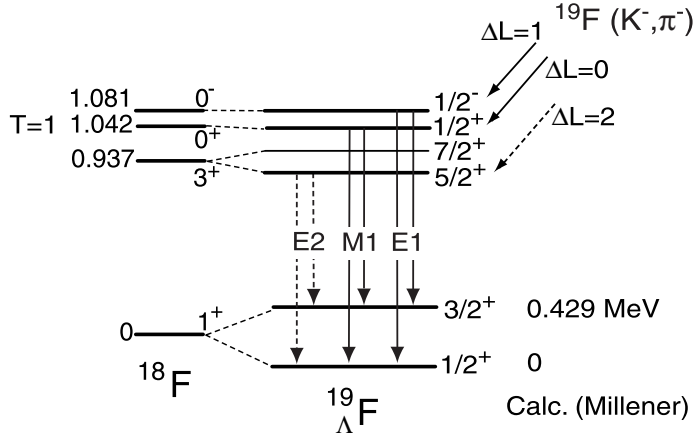


Figure 10: Expected level scheme of  $^{19}\text{F}$ . Transitions expected to be observed in the proposed experiment are also shown.

But the distance between the  $\Lambda$  in the  $0s$  orbit and nucleons in the  $d$  orbit in  $sd$ -shell hypernuclei is different from the distance between the  $\Lambda$  in the  $0s$  orbit and nucleons in the  $p$  orbit in  $p$ -shell hypernuclei. Therefore, the spin-spin interaction strength in  $^{19}\text{F}$  provides information on radial dependence of the  $\Lambda N$  spin-spin interaction, namely, the shape of  $V_\sigma(r)$  in Eq.2.

Here the contamination of  $^{12}\text{C}$  target causes no problem, because the  $^{12}\text{C}$   $\gamma$  rays less than 2 MeV are not expected to be emitted except for the spin-flip  $M1$  transition between the ground-state doublet ( $2^-, 1^-$ ). Therefore, both  $^{19}\text{F}$   $M1(1/2^+ \rightarrow 3/2^+, 1/2^+)$  transitions as well as the  $3/2^+ \rightarrow 1/2^+$  spin-flip transition can be observed and discriminated from the  $^{12}\text{C}$   $\gamma$  rays.

## 2.5 $^4_\Lambda\text{He}$

In the proposed experiment, we measure the ground-state doublet spacing ( $1^+, 0^+$ ) of  $^4_\Lambda\text{He}$  using a liquid helium target. The  $M1$  transition  $\gamma$  ray of  $^4_\Lambda\text{He}$  ( $1^+ \rightarrow 0^+$ ) was measured several times with NaI counters and the doublet ( $1^+, 0^+$ ) spacing was determined to be  $1.08 \pm 0.02$  MeV (see Fig. 11). On the other hand, the measurement of  $^4_\Lambda\text{He}$   $\gamma$  rays was once reported in 1970's, claiming the  $^4_\Lambda\text{He}$  ( $1^+ \rightarrow 0^+$ ) energy of  $1.15 \pm 0.04$  MeV. Since the statistical quality of the  $^4_\Lambda\text{He}$   $\gamma$  ray spectrum is extremely poor, as shown in Fig. 12, it has to be measured again with the modern technique. In the proposed experiment, we can easily measure the spacing energy of  $^4_\Lambda\text{He}(1^+ \rightarrow 0^+)$  precisely.

There is another important objective in the  $^4\text{He}$  target run. The cross sections of  $\Lambda$  hypernuclear productions by  $(K^-, \pi^-)$  reaction on a nucleus, particularly their spin-flip and non-spin-flip cross sections (or polarization properties), for the  $K^-$  momentum higher than 1 GeV/ $c$  are not measured yet, although they are important for further studies of hypernuclear physics at J-PARC. By using  $^4_\Lambda\text{He}$  hypernucleus, we can also measure the cross sections of the spin-flip  $1^+$  and non-flip  $0^+$  states by  $(K^-, \pi^-)$  reaction at several momenta (e.g. 1.3, 1.5, 1.8 GeV/ $c$ ) and confirm the theoretical calculations based on the elementary cross sections in Fig. 14. The  $(K^-, \pi^-)$  reaction in a nuclear matter is not completely understood due to hyperon resonances.

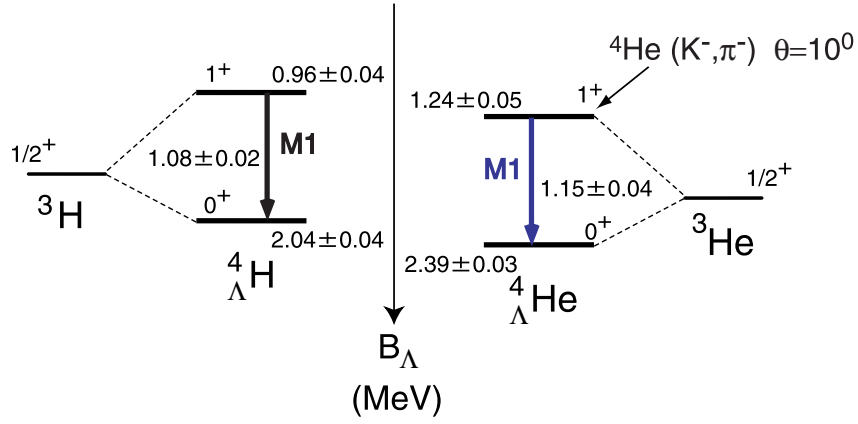


Figure 11: Level schemes of the mirror hypernuclei,  ${}^4_{\Lambda}\text{H}$  and  ${}^4_{\Lambda}\text{He}$ . A large charge symmetry breaking in the  $\Lambda N$  interaction is suggested.

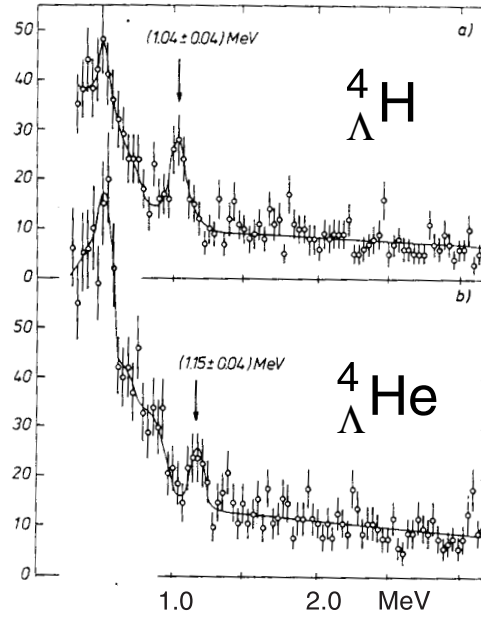


Figure 12: Level schemes of the mirror hypernuclei,  ${}^4_{\Lambda}\text{H}$  and  ${}^4_{\Lambda}\text{He}$  [30]. Statistical quality of the  ${}^4_{\Lambda}\text{He}$   $\gamma$ -ray peak is poor.

So the data will play an essential role to establish the  $(K^-, \pi^-)$  reaction mechanism and to make more realistic estimates of hypernuclear production in the future. For this purpose,  ${}^4_{\Lambda}\text{He}$  is the best hypernucleus because the cross sections for  $0^+$  and  $1^+$  are particularly large, and the  $1^+$  state is produced purely by the spin-flip interaction.

The absolute cross sections for  $1^+ + 0^+$  states are measured from the peak counts in the  $(K^-, \pi^-)$  spectrum. Although the  $1^+$  and  $0^+$  peaks are not separated, the  $1^+ \rightarrow 0^+$   $\gamma$ -ray yield provides the ratio of the  $1^+$  and  $0^+$  productions.

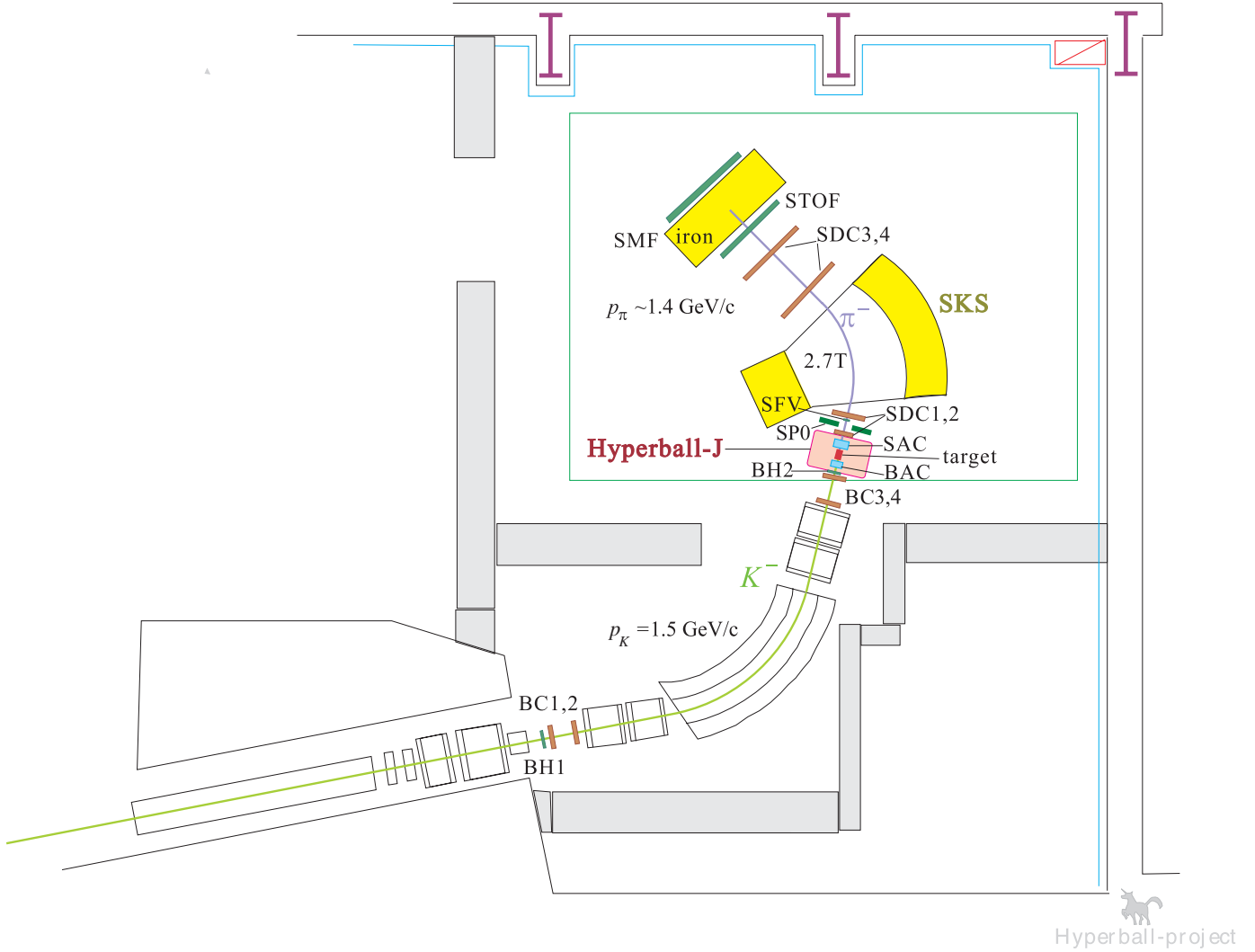


Figure 13: Experimental setup at the K1.8 beam line.

### 3 Experimental Setup

In the proposed experiment, we need to produce excited states of  $\Lambda$  hypernuclei via the  $(K^-, \pi^-)$  reaction at 1.1 GeV/c or 1.5 GeV/c employing the K1.1 or K1.8 beam line and SKS, and measure  $\gamma$  rays from the hypernuclei with the germanium detector array Hyperball-J. In this proposal, we design the experiment using the K1.8 beam line, because use of the K1.1 line is not realistic as a Day-1 experiment.

#### 3.1 Beam line

We use the  $(K^-, \pi^-)$  reaction to produce  $\Lambda$  hypernuclei. In many cases, one of the hypernuclear spin-doublet states (see Fig. 2) is produced from the target nucleus by the non-spin-flip ampli-

tude of the elementary reaction ( $K^-n \rightarrow \Lambda\pi^-$ ), and the other state of the doublet is produced by the spin-flip amplitude. Therefore, by using both spin-flip and non-spin-flip amplitudes, we can discriminate between the spin-flip and non-spin-flip states in the doublet, which gives essential information for reconstruction of the level scheme from observed  $\gamma$  rays.

Figure 14 shows the cross sections of the elementary reaction  $K^-n \rightarrow \Lambda\pi^-$  for the non-spin-flip interaction ( $|f|^2$ ) and for the spin-flip interaction ( $|g|^2$ ) as a function of  $K^-$  momentum. The spin-flip cross section is large at 1.1 to 1.45 GeV/ $c$ , while the non-spin-flip cross section is small in this momentum region. Therefore, in order to populate both spin-flip and non-spin-flip states without changing the experimental setup, the best  $K^-$  beam momentum is 1.1 GeV/ $c$  and 1.45 GeV/ $c$ . In both cases, we require the  $\pi/K$  ratio less than 0.5 to minimize the radiation damage to the Ge detectors.

Although in the K1.1 beam line the  $K^-$  intensity is optimized to 1.1 GeV/ $c$ , this beam line has not been funded yet. As a realistic solution, we will use the 1.5 GeV/ $c$  beam <sup>3</sup> from the K1.8 beam line which will be available for Day-1 experiments. In addition, we need a good spectrometer with a momentum resolution better than 0.2% FWHM to select the bound state region of hypernuclei. For this purpose, the SKS spectrometer which will be installed at the K1.8 beam line is best fitted. According to our simulation, SKS can be used for the ( $K^-, \pi^-$ ) reaction up to  $p_{K^-} = 1.5$  GeV/ $c$  ( $p_{\pi^-} \sim 1.4$  GeV/ $c$ ) without unacceptable degradation of the momentum resolution and the acceptance.

We may be able to use the K1.8BR beam line (maximum momentum of 1.1 GeV/ $c$ ), but the  $\pi/K$  ratio less than 0.5 will not be achieved because this line has a single-stage mass separator. In the ( $K^-, \pi^-$ ) reaction at 1.1 GeV/ $c$  beam, the  $\pi^-$  momentum is 1.0 GeV/ $c$ . It is higher than the maximum momentum for the SPES-II spectrometer (0.9 GeV/ $c$ ) which is planned to be used at the K1.8BR beam line. Therefore, we need to install the SKS at the K1.8BR beam line, which seriously conflicts with other experimental proposals.

### 3.2 Magnetic Spectrometers

Figure 13 shows the experimental setup at K1.8. It is similar to the previous setup for the ( $\pi^+, K^+$ ) reaction at the K6 beam line in KEK-PS, but some detectors are modified or introduced for the ( $K^-, \pi^-$ ) reaction. Those detectors were designed from our experience of using the ( $K^-, \pi^-$ ) reaction with the intense  $K^-$  beam (0.93 GeV/ $c$ ,  $0.2 \times 10^6$   $K^-$  per spill) at the AGS D6 beam line in the BNL E930 experiment.

The kaon beam momentum is analyzed by the K1.8 beam line spectrometer which is composed of the QQQ magnets, 1 mm pitch MWPC's (BC1, BC2) and 3 mm-pitch drift chambers (BC3, BC4), and timing counters (BH1, BH2). The  $\pi^-/K^-$  ratio of the beam is estimated to be 0.2 [33]. Since the MWPC's can accept the beam up to  $1 \times 10^6$  particles per wire and the beam size is more than a few cm, the total acceptable counting rate is much higher than the maximum available  $K^-$  beam intensity of  $0.5 \times 10^6$   $K^-$  per spill at 1.5 GeV/ $c$ ,<sup>4</sup> which is expected in the full-intensity proton beam (30 GeV, 9 $\mu$ A) before the Linac and PS energy

---

<sup>3</sup>Since  $K^-$  intensity at 1.5 GeV/ $c$  is 1.25 times larger than at 1.45 GeV/ $c$ , the use of 1.5 GeV/ $c$  beam is optimum.

<sup>4</sup>At BC1 and BC2, the counting rate is expected to be 10 times more than the beam intensity at the experimental target, but it is still acceptable for these MWPC's.

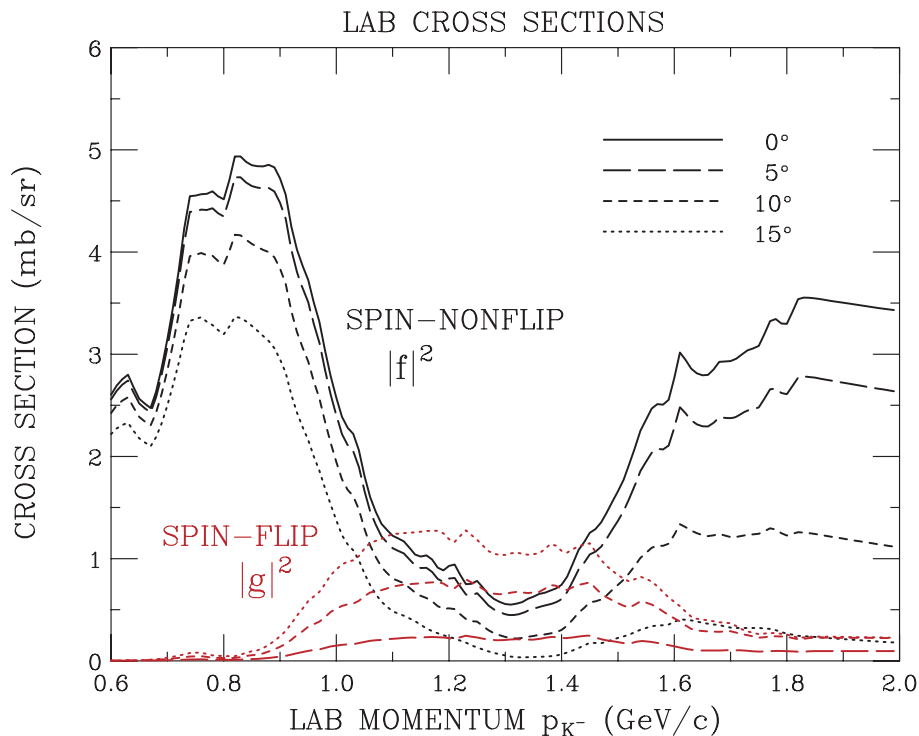


Figure 14: Non-spin-flip and spin-flip cross sections of the  $K^-n \rightarrow \Lambda\pi^-$  reaction as a function of  $K^-$  momentum [31, 32].

recovery. The momentum resolution of the K1.8 beam line spectrometer is estimated to be 0.014% in rms [33], which gives negligible effect to the energy resolution of the hypernuclear mass spectrum with our thick targets ( $\sim 20$  g/cm<sup>2</sup>).

The kaon beam is irradiated to various targets; liquid  $^4\text{He}$  (2.0 g/cm<sup>2</sup>),  $^{nat}\text{Li}_2\text{O}$  (17.2 g/cm<sup>2</sup> for  $^7\text{Li}$ )  $^{10}\text{B}$  metal (20 g/cm<sup>2</sup>),  $^{11}\text{B}$  metal (20 g/cm<sup>2</sup>), and  $^{19}\text{F}$  in teflon (15.2 g/cm<sup>2</sup> for  $^{19}\text{F}$ ). Just upstream and downstream of the target located are aerogel Cerenkov counters (BAC and SAC) to identify kaons in the beam and pions in the scattered particles. Unscattered beam particles are detected by the SFV counter, of which signal is used to veto the trigger.

The scattered pions are identified and momentum-analyzed by use of the SKS magnet, tracking chambers (SDC1-SDC4), and TOF stop counters (STOF). The SDC1,2 located upstream of the SKS magnet are 1 mm pitch MWPC's, and SDC3,4 located downstream of the SKS magnet are new drift chambers with 2.5mm drift length. Since the beam kaons (1.5 GeV/c) and the scattered pion (1.4 GeV/c) are not spatially well separated by the SKS magnet, some area in the SDC3,4 chambers should have a high counting rate due to the beam. We will fabricate new SDC3-4 chambers with XX'UU'VV' planes for each of SDC3 and SDC4, so that at least two pair planes should always have low counting rates except for the beam spot region. Each of them has a size of 2 m x 0.8 m, larger than the previous SDC3 and 4.

By exciting the SKS magnet to the maximum field (2.7 T), the SKS sustains an acceptance of about 100 msr in the present setup. Since the SKS covers a wide range of scattering angle ( $|\theta| < 20^\circ$ ), we can populate non-spin-flip states at  $|\theta| < 10^\circ$  and spin-flip states at  $|\theta| > 10^\circ$

simultaneously (see Fig. 5, for example). According to our simulation, the bending angle for 1.5 GeV/ $c$  beam is typically 60 degree, significantly smaller than the angle for the usual setting (100 degree). Then we expect to have a hypernuclear mass resolution of 4.1 MeV (FWHM) without energy loss effect in the target, which is mainly determined by the SKS resolution. Although it is much worse than the usual SKS experiments at KEK by the  $(\pi^+, K^+)$  reaction ( $\sim 2$  MeV (FWHM)), our mass resolution is mainly determined by the energy loss effect in the thick (typically 20 g/cm<sup>2</sup>) target. By including the energy loss effect, the mass resolution is estimated to be 5.9 MeV (FWHM), which is enough to tag the hypernuclear bound state region.

The  $(K^-, \pi^-)$  trigger is made as

$$Kin \times PIout = (BH1 \times BH2 \times \overline{BAC}) \times (SAC \times \overline{SFV} \times \overline{SP0} \times STOF \times \overline{SMF}).$$

According to our experience of BNL E930, however, the beam  $K^-$ 's which decay in flight between BAC and SAC (namely, in the target region) as  $K^- \rightarrow \mu^- \nu$  and  $\pi^- \pi^0$  make a serious background, not only in the trigger level but even after the full analysis of the hypernuclear mass, because  $\mu^-$  and  $\pi^-$  from  $K^-$  decay enter the same kinematical region (momentum and scattering angle) as the  $\pi^-$  associated with hypernuclear production. In order to reject muons, we install a set of muon filters (SMF) made of a 80 cm thick iron block and thin plastic counters behind it. According to a simulation, muons with 1.25–1.5 GeV/ $c$ , which causes serious background in the hypernuclear mass spectrum, can be completely detected by SMF and removed, and all the  $\pi^-$ 's associated with the hypernuclear production do not hit SMF. But the low momentum ( $< 1.25$  GeV/ $c$ ) muons which stop in the iron block remain in the trigger. As for the  $K^- \rightarrow \pi^- \pi^0$  and other  $\pi^0$  emitting decay modes, we can detect  $\pi^0$  by using a few layers of lead-plastic sandwiched counters which are installed between SDC1 and SDC2 and cover the forward angles except for the SKS entrance. A simulation showed that these  $\pi^0$  counters (SP0) reject 80% of the  $\pi^0$ -emitting  $K^-$  decays occurring at the target region.

In addition, we include the Ge detectors and the PWO counters (see below) into the trigger. Using FPGA modules, we will make the *Gamma* trigger by requiring that more than one Ge+PWO set have a valid hit (Ge hit without ADC overflow and no PWO hit in any of the surrounding PWO counters). This trigger technique has already been established in our experiments at Tohoku Cyclotron. It greatly reduces fake triggers from  $K^-$  decays, and the trigger rate is estimated from the E930 condition to be less than 500 per spill for the full beam intensity ( $0.5 \times 10^6 K^-/\text{spill}$ ).

### 3.3 Hyperball-J

The  $\gamma$  rays from hypernuclei are detected by Hyperball-J, a newly-constructed large germanium detector array dedicated to hypernuclear  $\gamma$  spectroscopy. It is an upgraded version of Hyperball (constructed in 1998, photo-peak efficiency  $\epsilon = 2.5\%$ ), and Hyperball2 (constructed in 2005, photo-peak efficiency  $\epsilon \sim 4.5\%$ ), which have been used for hypernuclear  $\gamma$  spectroscopy experiments.

Figure 15 illustrates Hyperball-J. It consists of about thirty sets of the new Ge detector having a relative photo-peak efficiency <sup>5</sup> of about 75%. Each Ge detector is surrounded by fast

<sup>5</sup>Relative to  $3''\phi \times 3''$  NaI detector.

PWO counters for background suppression instead of the previous BGO counters. The expected counting rate and energy deposit rate to the Ge detectors will be much lower than those in the previous experiments at KEK-PS using  $(\pi^+, K^+)$  reaction with  $3 \times 10^6$  pion beam, because we found in our BNL E930 experiment with  $(K^-, \pi^-)$  reaction that the counting and energy deposit rates of Ge detectors are roughly proportional to the total beam (kaon+pion) rate regardless of the particle species. Therefore, the fast readout electronics used in the present Hyperball2 will work fine under the beam intensity for the proposing Day-1 experiment ( $0.5 \times 10^6 K^-$  per spill (0.7 s)).<sup>6</sup>

As shown in Fig.15, the Ge detectors are arranged at top and bottom and the distance of each detector from the target can be adjusted according to the requirement of the experiment and beam conditions. In the proposed experiment, the detectors are installed about 15 cm from the target center.

Figure 16 shows the simulated photo-peak efficiency. According to a simulation, it is about 6.4% for a point source and 5.0% for the realistic source point distribution in the  $\text{Li}_2\text{O}$  target in the most conservative estimate. Detailed design work for Hyperball-J is in progress. By combining the old Ge detectors used in the previous Hyperball and Hyperball2, we will be able to increase the efficiency.

According to our experience, Ge detectors will suffer from radiation damage due to neutrons and pions – effects of damage begin to appear in one or two months' run under the pion beam intensity of  $3 \times 10^6$  per spill at the KEK-PS K6 beam line. By keeping the Ge crystal temperature lower ( $< 85$  K) than usual ( $\sim 90$ – $95$  K), the effect of radiation damage can be greatly reduced. Thus, we are now developing a stronger cooling method by using a mechanical refrigerator or a modified connection between the crystal and the liquid nitrogen Dewar. So we expect the radiation damage will be much less serious in Hyperball-J.

The PWO scintillator has a higher density and a larger effective atomic number than BGO and emits a light much faster (decay time  $\sim 10$  ns) than BGO ( $\sim 300$  ns). It is suitable for a high counting rate condition in the J-PARC experiments. Although the light output is much smaller than BGO, we can expect nearly 100% efficiency for 100 keV photons when PWO crystals are cooled down to  $-20^\circ$ . We have made a prototype of the PWO background suppressor and already confirmed their performance; the PWO suppressor is good enough for high energy  $\gamma$ -ray suppression, and as for the Compton suppression, the PWO suppressor also has a similar performance to our previous BGO suppressor as shown in Fig. 17.

---

<sup>6</sup>A new readout method based on waveform digitization is under development for more beam intensity in the future. But in the present full beam intensity for 30 GeV-9 $\mu$ A operation we do not need it.

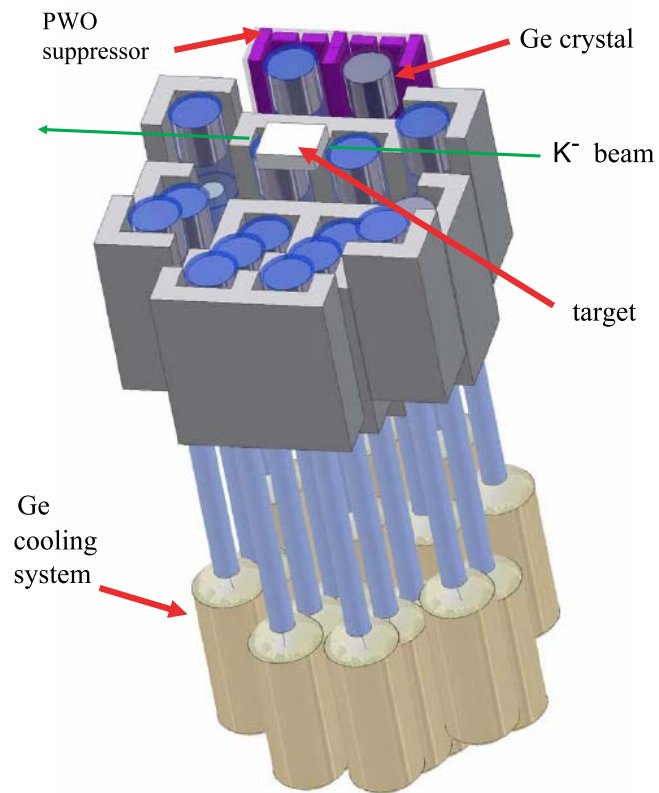
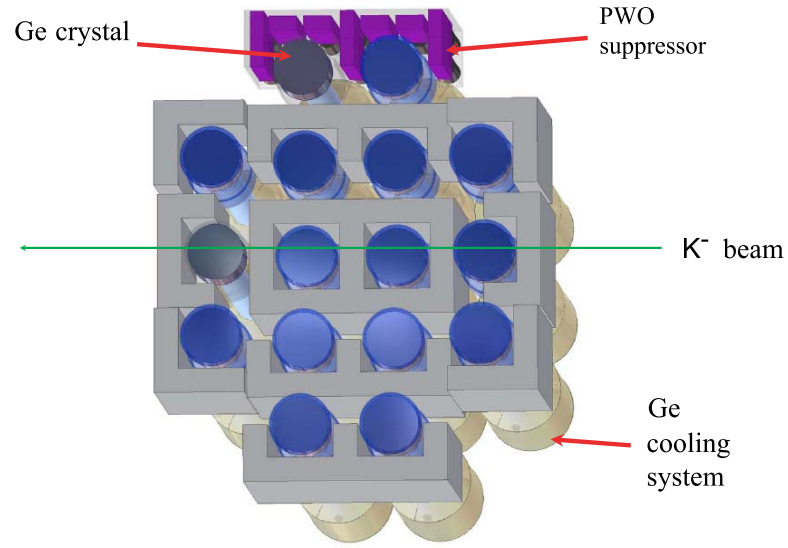


Figure 15: Schematic view of Hyperball-J (lower half only) viewed from top (top figure) and from side (bottom figure).

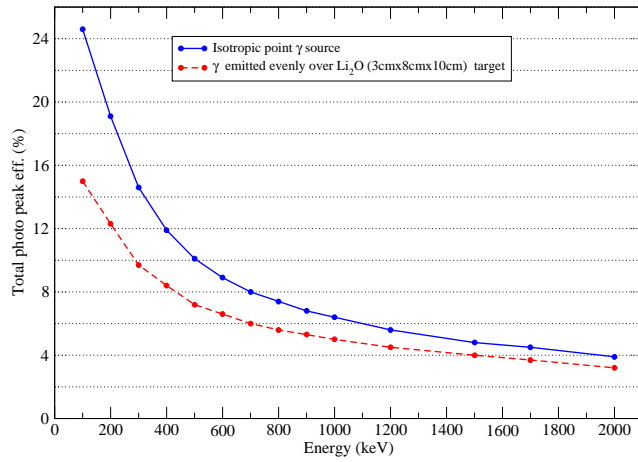


Figure 16: Simulated efficiency curve of Hyperball-J for a point source and for a realistic condition with source points distributed over the  $\text{Li}_2\text{O}$  target.

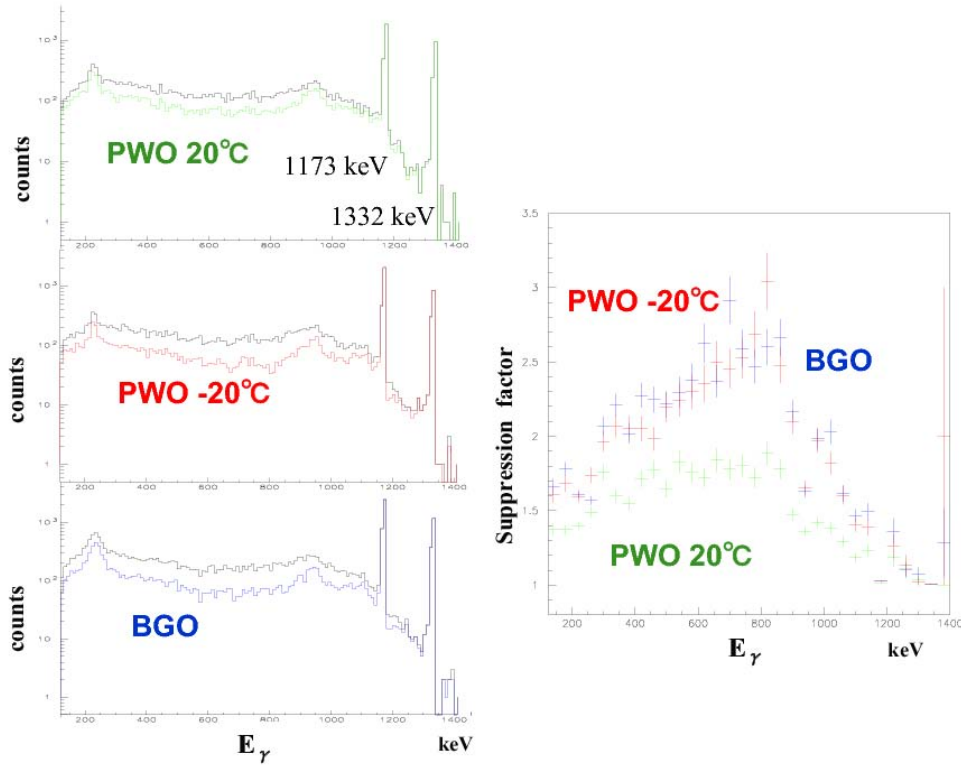


Figure 17: Compton suppression performance of prototype PWO counters (at room temperature and at  $-20^\circ\text{C}$ ) compared with BGO counters used in the previous Hyperball. Left:  $^{60}\text{Co}$   $\gamma$ -ray spectra before and after the suppression. Right: Suppression factor (the spectrum before suppression is divided by the spectrum after suppression).

## 4 Yield estimate and expected results

### 4.1 Experimental conditions

The conditions for the proposed experiment are summarized in Table 1.

Table 1: Experimental conditions of the proposed experiments.

<b>Reaction</b>	$(K^-, \pi^-)$
<b>Target</b>	$\text{Li}_2\text{O}, {}^{10}\text{B}, {}^{11}\text{B}, (\text{CF}_2)_n(\text{teflon}), {}^4\text{He}$
<b><math>\gamma</math>-ray detector</b>	Hyperball-J
<b>Efficiency</b>	6 %@ 1 MeV $\gamma$ ray
<b>Ge live time</b>	0.7
<b>Beam line</b>	K1.8
<b>Beam momentum</b>	1.5 GeV/ $c$
<b>Beam intensity</b>	$0.5 \times 10^6 K^-$ per spill @ primary 30 GeV/ $c$ , $9\mu\text{A}$
<b>Beam size @Final focus</b>	46.5/7.5 mm (FWHM)
<b>Forward Spectrometer</b>	SKS with SDC3,4 and muon filter
<b>SKS coverage</b>	$\pm 20^\circ$ (horizontal), $\pm 5^\circ$ (vertical)
<b>SKS acceptance</b>	100 % ( $5^\circ$ ), 35 % ( $10^\circ$ )
<b><math>\pi^-</math> detection angle</b>	$< 10^\circ$ for non-spin-flip, $> 10^\circ$ for spin-flip
<b>Trigger</b> $K_{in} \times P_{Iout} \times \text{Gamma}$	
<b><math>K_{in}</math> trigger</b>	$BH1 \times BH2 \times \overline{BAC}$
<b><math>P_{Iout}</math> trigger</b>	$SAC \times \overline{SFV} \times \overline{SP0} \times \overline{STOF} \times \overline{SMF}$
<b><math>\text{Gamma}</math> trigger</b>	$\Sigma_i(\text{Ge}_i \times \overline{PWO}_i)$

### 4.2 ${}^7_\Lambda\text{Li}$

Table 2 shows the expected  $\gamma$ -ray yield in the  ${}^7_\Lambda\text{Li}$  experiment. Figure 18 shows a simulated spectrum around the  ${}^7_\Lambda\text{Li}$  ( $3/2^+ \rightarrow 1/2^+$ )  $\gamma$  ray for 500 hours' run with  $0.5 \times 10^6 K^-$  per spill. In this simulation, the lifetime of the  $3/2^+$  state is assumed to be 0.5 ps, which corresponds to the  $B(M1)$  value when  $g_\Lambda$  is unchanged from the free-space value.

The background in the simulated spectrum was reliably estimated from our  ${}^7_\Lambda\text{Li}$   $\gamma$ -ray spectrum measured in KEK E419, in which background contribution from the  ${}^{16}\text{O}(K^-, \pi^-)$  reaction is also included. By fitting the peak with simulated peak shapes for various lifetimes, the lifetime of the  $3/2^+$  state was obtained to be  $0.478 \pm 0.026$  ps, demonstrating a statistical accuracy of the proposed  $B(M1)$  measurement. Thus, we expected to determine the lifetime of the  $3/2^+$  state within 5.4% accuracy. It corresponds to a statistical error of 3% for  $|g_\Lambda - g_c|$ . According to our experience in the  $B(E2)$  measurement of  ${}^7_\Lambda\text{Li}$  (KEK E419) [2], the systematic error is

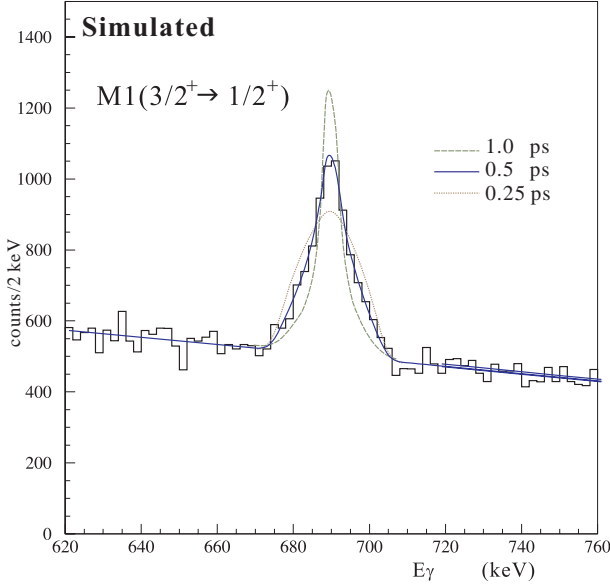


Figure 18: Simulated  $\gamma$ -ray spectrum to be measured in the  ${}^7\text{Li}(K^-, \pi^-){}_\Lambda^7\text{Li}$  reaction with reaction angles from  $2.5^\circ$  to  $5^\circ$ . The partly-Doppler-broadened peak is the spin-flip  $M1(3/2^+ \rightarrow 1/2^+)$  transition in  ${}^7_\Lambda\text{Li}$  assuming the lifetime of the  $3/2^+$  state to be 0.5 ps. The simulated  $\gamma$ -ray yield, 3600 counts, corresponds to the 500 hours beam time. By fitting this peak with a simulated shape, the lifetime was derived to be  $0.478 \pm 0.027$  ps, demonstrating a statistical accuracy of the proposed  $B(M1)$ .

estimated to be less than 5%; the systematic error here is mainly from inaccuracy of the stopping time calculation, and the effect of possible alignment of hypernuclei, which was another main source of the systematic error in E419, does not exist here because of the  $1/2^+(T = 1)$  spin of the populated  ${}^7_\Lambda\text{Li}$  level.

The other spin-flip  $M1$  transition ( $7/2^+ \rightarrow 5/2^+$ ) was previously observed at 471 keV [7]. The spin-flip  $B(M1)$  of this transition can be also measured in this experiment. However, there exists a background peak of  ${}^7\text{Li}$  at 478 keV, which can not be eliminated from the spectrum; it is Doppler-broadened and expected to give a serious effect in the determination of the  ${}^7_\Lambda\text{Li}(7/2^+)$  lifetime from the 471-keV peak shape.

On the other hand, the  $E2(7/2^+ \rightarrow 3/2^+)$  transition at 1829 keV can be used to determine the lifetime of the  $7/2^+$  state. Although the branching ratio of this transition is small, estimated to be 17% and measured to be  $<19\%$ , we expect to have 500 counts in 500 hours. Figure 19 shows a simulated spectrum around the 1829 keV peak assuming a lifetime of 1.7 ps, plotted after a tight  $\pi^-$  scattering angle selection. As shown in the figure, a fitted result was  $1.53^{+0.52}_{-0.32}$  ps. So we can determine the  $B(M1)(7/2^+ \rightarrow 5/2^+)$  in 26% error. <sup>7</sup>

### 4.3 ${}^{10}_\Lambda\text{B}$ , ${}^{11}_\Lambda\text{B}$ , and ${}^{19}_\Lambda\text{F}$

Table 3 shows the expected yields of relevant  $\gamma$  transitions in the  ${}^{10}_\Lambda\text{B}$  and  ${}^{19}_\Lambda\text{F}$  experiments.

For the  ${}^{10}_\Lambda\text{B}$  experiment, the  $M1(2^- \rightarrow 1^-)$   $\gamma$ -ray yield is estimated to be 38 counts/hour when  $E(2^-) - E(1^-) = 100$  keV, but the yield goes down for lower transition energy, to 20 counts/hour for 50 keV, due to competition with weak decay and  $\gamma$ -ray absorption loss in the target material. In 100 hours we can collect data with about 10 times more statistics than the previous  ${}^{10}_\Lambda\text{B}$  experiment in BNL E930('01) [5]. Figure 20 shows simulated spectra demonstrating the peak count and the background for the  ${}^{10}_\Lambda\text{B}$   $M1(2^- \rightarrow 1^-)$  or  $M1(1^- \rightarrow 2^-)$

<sup>7</sup>Since the branching ratio for the  $7/2^+ \rightarrow 5/2^+$  transition ( $\sim 0.83$ ) will be obtained with a negligibly small error ( $\sim 1\%$ ), the  $B(M1)$  error stems from the lifetime error.

Table 2: Expected  $\gamma$ -ray yields for the  ${}^7_\Lambda\text{Li}$  experiment.

$J_i^\pi$	$1/2^+, 1$	$7/2^+$	$5/2^+$	$3/2^+$
$E_x$ (keV)	3877	2521	2050	692
$\tau$ (ps) exp.			$5.8 \pm 1.5$	$0.3 \sim 2.0$
$\tau$ (ps) calc.		1.7		0.5
$J_f^\pi$	$3/2^+, 1/2^+$	$5/2^+, 3/2^+$	$3/2^+, 1/2^+$	$1/2^+$
$EM\lambda$	M1, M1	M1, E2	E2, E2	M1
$E_\gamma$ (keV)	3185, 3877	471, 1829	1358, 2050	692
$\varepsilon_\gamma$ (%)y		7.5, 3.5	4.1, 3.1	6.0
Branch exp.	100, 100	100, <19	<4, 100	100
Branch calc.		100, 17	4, 100	
$d\sigma/d\Omega@5^\circ$ ( $\mu\text{b}/\text{sr}$ )	13.95	1.94	23.75	2.68
$d\sigma/d\Omega@10^\circ$ ( $\mu\text{b}/\text{sr}$ )	6.83	5.13	13.21	7.10
$\int_{2.5^\circ}^{5.0^\circ} d\sigma/d\Omega \cdot \delta\Omega \times \text{Branch}$ ( $\mu\text{b}$ )	<b>0.257</b> , 0.257	0.046, 0.008	0.034, 0.843	<b>0.074</b>
$\int_{2.5^\circ}^{20^\circ} d\sigma/d\Omega \cdot \delta\Omega \times \text{Branch}$ ( $\mu\text{b}$ )	0.844, 0.844	<b>0.579</b> , <b>0.098</b>	0.111, 2.763	0.937
Target	$0.86 \text{ g}/\text{cm}^3 \times 20 \text{ cm} \times 6.02 \times 10^{23}/7 = 14.8 \times 10^{23} / \text{cm}^2$			
$N_{K^-}$ / hour	$0.5 \times 10^6 / \text{spill} \times 1000 \text{ spill} / \text{hour} = 5 \times 10^8$			
Ge livetime	0.7			
SKS efficiency	0.6			
Yield /hour/ $\mu\text{b}$	$3.108 \times 10^2$			
$\int_{2.5^\circ}^5 \gamma\text{-ray counts}/\text{hour}$ (w/o feeding)				1.38
$\int_{2.5^\circ}^5 \gamma\text{-ray counts}/\text{hour}$ (w/ feeding)				<b>7.30</b> +0.97 <sup>1)</sup>
$\int_{2.5^\circ}^{20^\circ} \gamma\text{-ray counts}/\text{hour}$		<b>13.5</b> , <b>1.09</b>	1.41, 32.2	
$\int_{2.5^\circ}^{20^\circ} \gamma\gamma$ coin counts/hour		<b>0.39</b> <sup>2)</sup> , 0.06 <sup>2)</sup>		

1) Cascade decay via the upper slow states ( $7/2^+, 5/2^+$ )

2) Coincident with the  $5/2^+ \rightarrow 1/2^+$  transition

$\gamma$  rays. If the ordering of ( $2^-, 1^-$ ) is reversed (right figure), the  $\gamma$ -ray yield decreases by a factor of 7–8 due to a lower cross section of the spin-flip state. Nevertheless, we will be able to detect the  $1^- \rightarrow 2^-$  transition in 100 hours when the spacing is larger than 50 keV.

For the  ${}^{19}_\Lambda\text{F}$  experiment, we need to take angular distribution of the ( $K^-, \pi^-$ ) reaction for  $\gamma$ -ray events to identify  $\Delta L$  and assign the transitions. The S/N ratio in the  $\gamma$ -ray spectrum will be worse than  $p$ -shell hypernuclei. So we request 100 hours which corresponds to at least 1200 counts for the  $1/2^- \rightarrow 1/2^+, 3/2^+$  transitions.

Table 4 shows the expected yields of relevant  $\gamma$  transitions in the  ${}^{11}_\Lambda\text{B}$  experiment. Here the cross sections of various  ${}^{11}_\Lambda\text{B}$  states were calculated by Motoba [15]. The yields for several  $\gamma\gamma$  coincidence measurements, which are necessary to reconstruct the level scheme, are also

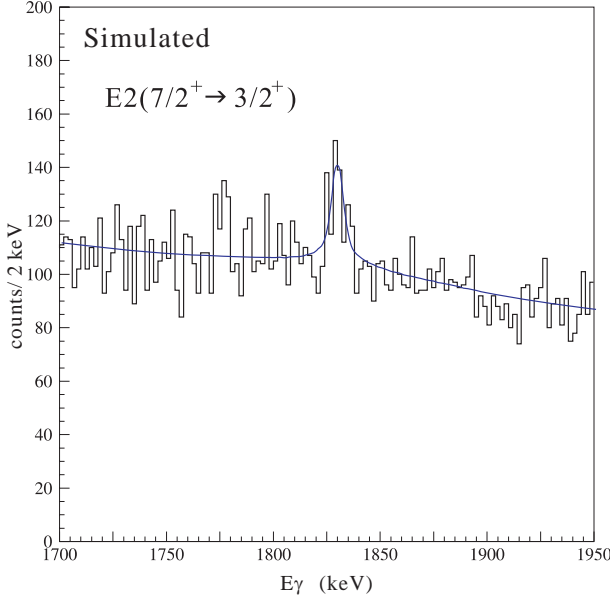


Figure 19: Simulated  $\gamma$  ray spectrum to be measured in the  ${}^7\text{Li}(K^-, \pi^-){}_\Lambda^7\text{Li}$  reaction with reaction angles from  $7.5^\circ$  to  $20^\circ$ . The partly-Doppler-broadened peak is the  $E2(7/2^+ \rightarrow 3/2^+)$  transition in  ${}_\Lambda^7\text{Li}$ , in which the lifetime of the  $7/2^+$  state is assumed to be 1.7 ps.

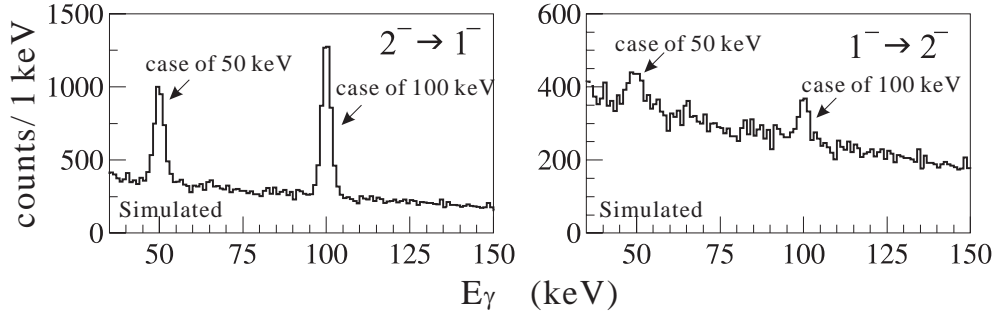


Figure 20: Simulated  $\gamma$ -ray spectrum in the  ${}^{10}\text{B}(K^-, \pi^-){}_\Lambda^{10}\text{B}$  reaction. The ground-state doublet spacing was found to be  $E(2^-) - E(1^-) < 100$  keV in the previous experiments [26, 5]. In this simulation the spacing is assumed to be 50 keV and 100 keV. The simulated peaks for these two cases are shown together in one figure. Left figure (right figure) shows the case that the  $2^-$  state (the  $1^-$  state) is the upper member of the doublet. The number of simulated peak counts corresponds to the beam time of 100 hours.

shown. Thus, in 200 hours we will be able to obtain at least 16  $\gamma\gamma$  coincidence events for all the important transitions. The yields of the  $\gamma\gamma$  coincidence events are expected to be about 10 times larger than the previous KEK E518 experiment via the  $(\pi^+, K^+)$  reaction.

#### 4.4 ${}_\Lambda^4\text{He}$

Table 5 shows the expected counts for  ${}_\Lambda^4\text{He}(1^+)$  and  ${}_\Lambda^4\text{He}(0^+)$  peaks in the  $(K^-, \pi^-)$  spectrum and the  $1^+ \rightarrow 0^+$   $\gamma$ -ray counts for various  $K^-$  momenta. Although the two peaks cannot be separated in the mass spectrum, we can extract the cross sections of both states by combining the yield of the  $1^+ \rightarrow 0^+$   $\gamma$  rays. In order to obtain 200 counts of  $1^+ \rightarrow 0^+$   $\gamma$  ray we need about

Table 3: Expected yields for  ${}^{10}_{\Lambda}\text{B}$  and  ${}^{19}_{\Lambda}\text{F}$  experiments. Cross sections for the  ${}^{10}_{\Lambda}\text{B}$  ground-state doublet states were calculated by Motoba [15] and that for  ${}^{19}_{\Lambda}\text{F}(1/2^-)$  was roughly estimated from a calculated  ${}^{20}_{\Lambda}\text{Ne}(1^-)$  cross section [19].

Hypernucleus	${}^{10}_{\Lambda}\text{B}$		${}^{19}_{\Lambda}\text{F}$	
	$2^-$	$1^-$	$1/2^-$	
Populated state	$2^-$	$1^-$	$1/2^-$	
$P_{K^-}$ (GeV/c)	1.5			
$\int_{2.4^\circ}^{20^\circ} d\sigma/d\Omega \cdot \delta\Omega$	2.1 $\mu\text{b}$	0.23 $\mu\text{b}$	$\sim 40 \mu\text{b} \times 0.05 \text{ sr} = 5 \mu\text{b}$	
Target	$20 \text{ g/cm}^2 \times 6.02 \times 10^{23} / 10$		$15.2 \text{ g/cm}^2 \times 6.02 \times 10^{23} / 19$	
$N_{K^-}$ /hour	$0.5 \times 10^6 / \text{spill} \times 1000 \text{ spill/hour} = 5 \times 10^8$			
SKS efficiency	0.6			
Transition	$2^- \rightarrow 1^-$	$1^- \rightarrow 2^-$	$1/2^- \rightarrow 1/2^+$	$1/2^- \rightarrow 3/2^+$
$E_\gamma$ (MeV)	0.05–0.1	0.05–0.1	1.1	0.65
$\epsilon_\gamma$	0.13–0.15		0.06	0.08
Ge livetime	0.7			
$\gamma$ /[weak+ $\gamma$ ] branch	0.30–0.48	0.41–0.39		
$\gamma$ -ray counts /hour	20–38	3.0–4.2	12	16

30–10 hours for each momentum. Figure 21 shows simulated spectrum of the  ${}^4_{\Lambda}\text{He}$   $\gamma$  rays for 1.1, 1.3, 1.5, 1.8 GeV/c  $K^-$  after the event-by-event Doppler shift correction. The background was reliably estimated from the calculated production ratio of the  $0^+$  and  $1^+$  states and the  $\gamma$ -ray background per hypernuclear bound-state events measured for  ${}^7_{\Lambda}\text{Li}$  in KEK E419. Thus we can determine the  $1^+ - 0^+$  energy spacing in a few keV accuracy, and measure the cross section of each state within 10% accuracy.

## 5 Beam time request

The requesting beam time for each target is summarized in the following table. The main objective and physics motivation are also listed.

Target	(g/cm <sup>2</sup> )	Beam time	Main objective	Purposes
tuning		300 hrs		
${}^{nat}\text{Li}_2\text{O}$	(17.2 for ${}^7\text{Li}$ )	500 hrs	${}^7_{\Lambda}\text{Li}: B(M1:3/2^+ \rightarrow 1/2^+)$	$g_\Lambda$ in nucleus
${}^{10}\text{B}$ metal	(20)	100 hrs	${}^{10}_{\Lambda}\text{B}: E(2^-, 1^-)$	$\Lambda N$ spin dependence, $\Sigma\Lambda$ coupling
${}^{11}\text{B}$ metal	(20)	200 hrs	${}^{11}_{\Lambda}\text{B}$ : level scheme	$\Lambda N$ spin dependence, $\Sigma\Lambda$ coupling
$(\text{CF}_2)_n$ teflon	(15.2 for ${}^{19}\text{F}$ )	100 hrs	${}^{19}_{\Lambda}\text{F}: E(3/2^+, 1/2^+)$	$\Lambda N$ spin-spin int. in sd shell
He liquid	(3.13)	100 hrs	${}^4_{\Lambda}\text{He}: E(1^+, 0^+)$	$\Lambda N$ CSB, $(K^-, \pi^-)$ reaction test

Beam time is calculated for the  $K^-$  beam intensity of  $0.5 \times 10^6 K^-$  (1.5 GeV/c) per spill, which corresponds to 30 GeV, 9  $\mu\text{A}$  proton beam.

Table 4: Expected yields for  ${}_{\Lambda}^{11}\text{B}$  experiment.

Hypernucleus populated state	${}_{\Lambda}^{11}\text{B}$				
	$1/2_1^+$	$3/2_1^+$	$1/2^+(T=1)$	$3/2_2^+$	$3/2^+(T=1)$
$p_{K^-}$ (GeV/c)	1.5				
$\int_{2.5^\circ}^{20^\circ} d\sigma/d\Omega$ ( $\mu\text{b}$ )	0.54	0.21	0.69	1.4	1.8
Target	$20 \text{ g/cm}^2 \times 6.02 \times 10^{23}/11 = 1.1 \times 10^{24}$				
$N_{K^-}$ / hour	$0.5 \times 10^6/\text{spill} \times / \text{hour} = 5 \times 10^8$				
SKS efficiency	0.6				
transition	$1/2_1^+ \rightarrow 5/2_1^+$	$3/2_1^+ \rightarrow 1/2_1^+$	$1/2^+; 1 \rightarrow 1/2_1^+$	$3/2_2^+ \rightarrow 1/2_1^+$	$3/2^+; 1 \rightarrow 1/2_2^+$
$E_\gamma$ (MeV)	1.48	0.65	1.07	1.31	2.48
$\epsilon_\gamma$	0.040	0.063	0.050	0.043	0.027
Ge livetime	0.7				
BR	0.44				
$\gamma$ -ray counts/hour (cascade not included)	4.5	2.8	7.2	13	4.5
$\gamma$ - $\gamma$					
$\gamma(1)$		$3/2_1^+ \rightarrow 1/2_1^+$	$1/2^+; 1 \rightarrow 1/2_1^+$	$3/2_2^+ \rightarrow 1/2_1^+$	$1/2_2^+ \rightarrow 3/2_2^+$
$\gamma(2)$		$1/2_1^+ \rightarrow 5/2_1^+$	$1/2_1^+ \rightarrow 5/2_1^+$	$1/2_1^+ \rightarrow 5/2_1^+$	$1/2_2^+ \rightarrow 3/2_2^+$
$\gamma$ - $\gamma$ coin. counts/hour		0.08	0.20	0.36	0.13

## 6 Cost, manpower and time schedule

### 6.1 Hyperball-J

The new Ge detector array, Hyperball-J, is under construction in Tohoku University since 2005 with the Grant-in-Aid (spokesperson: H. Tamura, 2005–2009) of about 300 M yen. The grant covers the new Ge and PWO detectors and their cooling system, the support frame, the readout electronics and cables, and the data acquisition system.<sup>8</sup> Together with new Ge detectors purchased by this budget, Hyperball-J also includes the old Ge detectors and the readout electronics used in our previous devices, Hyperball and Hyperball2 (property of Tohoku University, 200 M yen in total) after some repairs and modifications. The construction and installation of Hyperball-J will be finished by the end of 2008. Hyperball-J will be also used in two proposed experiments by the  $(K^-, K^+)$  reaction to measure  $\Xi$ -atomic X rays [34, 35].

### 6.2 K1.8/SKS detectors

The K1.8 beam line and the SKS spectrometer system will be prepared by the beam channel group and the SKS group at KEK. Our experimental group will also join the construction of the detectors and the data-taking system for the K1.8/SKS spectrometers.

<sup>8</sup>But the air conditioning of the area,  $\sim 10$  NIM power bins, and some NIM modules are to be supported by KEK.

Table 5: Expected counts for  ${}^4_{\Lambda}\text{He}(1^+) + {}^4_{\Lambda}\text{He}(0^+)$  peak in the  $(K^-, \pi^-)$  spectrum and the  $1^+ \rightarrow 0^+$   $\gamma$ -ray counts in the  ${}^4_{\Lambda}\text{He}$  experiment for various  $K^-$  momenta. The cross sections are calculated by Harada [32].

Hypernucleus	${}^4_{\Lambda}\text{He}$							
	1.1		1.3		1.5		1.8	
$p_{K^-}$	1 <sup>+</sup>	0 <sup>+</sup>	1 <sup>+</sup>	0 <sup>+</sup>	1 <sup>+</sup>	0 <sup>+</sup>	1 <sup>+</sup>	0 <sup>+</sup>
$d\sigma/d\Omega@5^\circ$ ( $\mu\text{b}/\text{sr}$ )	25.36	892.46	49.15	238.28	39.74	195.18	15.68	344.19
$d\sigma/d\Omega@10^\circ$ ( $\mu\text{b}/\text{sr}$ )	61.42	193.13	46.74	42.27	19.28	36.88	3.17	18.30
$d\sigma/d\Omega@15^\circ$ ( $\mu\text{b}/\text{sr}$ )	28.92	23.98	9.01	2.51	1.10	0.64	0.01	0.00
$\int_{2.4^\circ}^{20^\circ} d\sigma/d\Omega \cdot \delta\Omega$ ( $\mu\text{b}$ )	8	90	6.5	24	5	20	2	34
Target	$0.125 \text{ g/cm}^3 \times 25 \text{ cm} \times 6.02 \times 10^{23}/4 = 4.7 \times 10^{23} /\text{cm}^2$							
$N_{K^-}/\text{spill} (\times 10^6)$	0.08		0.2		0.5		1.4	
$N_{K^-}/\text{hour}$	$\times 1000 \text{ spill/hour}$							
SKS efficiency	0.6							
Yield/hour/ $\mu\text{b}$	23		56		141		395	
${}^4_{\Lambda}\text{He}$ mass peak counts /hour	180	2070	360	1340	700	2800	790	13400
$\epsilon_\gamma$	0.05							
Ge livetime	0.7							
$\gamma$ -ray counts /hour	6		13		24		28	

The large-area high-rate drift chambers (SDC3 and SDC4), the muon filters, and aerogel Cerenkov counters around the target are needed particularly for this experiment. They will be constructed by manpower in Tohoku University and other colleagues in the Hyperball collaboration. These detectors will cost about 60 M yen. Since they can be also used for other proposed experiments at K1.8 and are also necessary for future experiments using  $(K^-, \pi^-)$  reaction at K1.8, we hope them to be financially supported by KEK. If they cannot be covered by KEK, we ask some contribution from collaborators abroad and also use our Grant-in-Aid budget by reducing the number of new Ge detectors in Hyperball-J.

### 6.3 Time schedule

Figure 22 shows the time schedule of the preparation for the proposed experiment. All the detectors will be ready by the end of 2008, when the first beam is expected to be delivered.

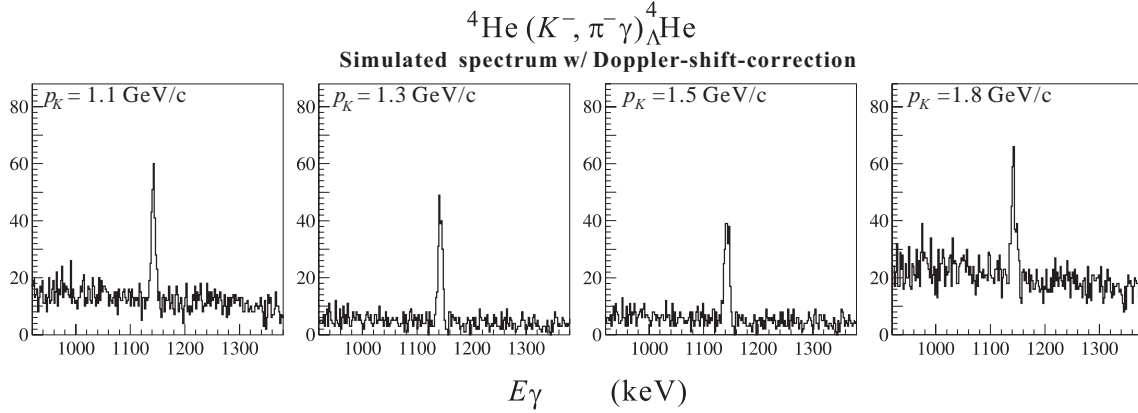


Figure 21: Simulated  $\gamma$ -ray spectrum in the  ${}^4\text{He} (K^-, \pi^-)$  reaction with  $K^-$  momenta of 1.1, 1.3, 1.5 and 1.8 GeV/c. Each figure shows the  $\gamma$ -ray spectrum after the event-by-event Doppler-shift correction.  $\gamma$ -ray yield of each peak is fixed to be 200 counts.

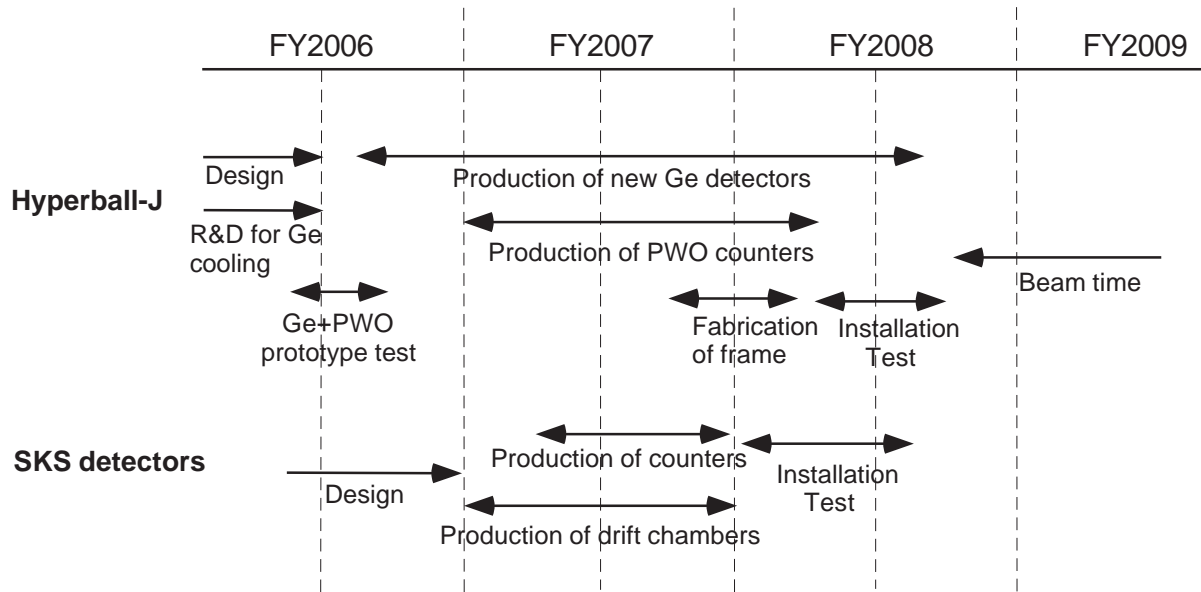


Figure 22: Schedule of the preparation for the proposed experiment.

## References

- [1] H. Tamura *et al.*, Phys. Rev. Lett. **84**, 5963 (2000).
- [2] K. Tanida *et al.*, Phys. Rev. Lett. **86**, 1982 (2001).
- [3] H. Akikawa *et al.*, Phys. Rev. Lett. **88**, 082501 (2002).
- [4] M. Ukai *et al.*, Phys. Rev. Lett. **93** (2004) 232501.
- [5] H. Tamura *et al.*, Nucl. Phys. A754 (2005) 58c.
- [6] Y. Miura *et al.*, Nucl. Phys. A754 (2005) 75c.
- [7] M. Ukai *et al.*, Phys. Rev. C73 (2006) 012501.
- [8] K. Imai *et al.*, Letter of Intent for Nuclear and Particle Physics Experiments at the J-PARC, KEK, L06 (2003), <http://www-ps.kek.jp/jhf-np/L0Ilist/L0Ilist.html>
- [9] E.V. Hungerford and L.C. Biedenharn, Phys. Lett. **142B** (1984) 232; T. Yamazaki, Nucl. Phys. **A 446** (1985) 467c.
- [10] T. Takeuchi, K. Shimizu, K.Yazaki, Nucl. Phys. **A 481** (1988) 693.
- [11] M. Asakawa *et al.*, Expression of Interest for Nuclear/Hadron Physics Experiments at the 50-GeV Proton Synchrotron, KEK Report 2000-11 (2000).
- [12] T. R. Saito *et al.*, Letter of Intent to GSI (2005).
- [13] R.H. Dalitz and A. Gal, Ann. Phys. **116** (1978) 167; J. Phys. G **6** (1978) 889.
- [14] K. Saito, M. Oka, T. Suzuki, Nucl. Phys. **A 625** (1997) 95;  
M. Oka, K. Saito, K. Sasaki, T. Inoue, “*Hadrons and Nuclei*” ed. Il-T. Cheon *et al.*, American Institute of Physics (2001) p.163.
- [15] T. Motoba, private communication (2006).
- [16] E. Hiyama, M. Kamimura, K. Miyazaki and T. Motoba, Phys. Rev. **C 59** (1999) 2351.
- [17] S. Ajimura *et al.*, Phys. Rev. Lett. **86** (2001) 4255.
- [18] E. Hiyama, M. Kamimura, T. Motoba, T. Yamada, Y. Yamamoto, Phys. Rev. Lett. **85** (2000) 270.
- [19] D.J. Millener, A. Gal, C.B. Dover, R.H. Dalitz, Phys. Rev. **C 31** (1985) 499.
- [20] M. M. Nagels *et al.*, Phys. Rev. D **15** (1977) 2547; Phys. Rev. D **20** (1979) 1633;  
P. M. Maessen *et al.*, Phys. Rev. C **40** (1989) 2226; Th.A. Rijken, V.G.J. Stokes and Y. Yamamoto, Phys. Rev. C **59** (1999) 21.
- [21] Y. Akaishi *et al.*, Phys. Rev. Lett. **84** (2000) 3539.

- [22] H. Nemura, Y. Akaishi, Y. Suzuki, Phys. Rev. Lett. **89** (2002) 142504.
- [23] E. Hiyama et al., Phys. Rev. **C66** (2002) 024007.
- [24] A.R. Bodmar and Q.N. Usmani, Phys. Rev. **C 31** (1985) 1400.
- [25] E. Hiyama, private communication (2006).
- [26] R.E. Chrien *et al.*, Phys. Rev. **C 41** (1990) 1062.
- [27] D.J. Millener, Nucl. Phys. **A754** (2005) 48c.
- [28] D.J. Millener, private communication (2006).
- [29] H. Bhang *et al.*, Phys. Rev. Lett. **81** (1998) 4321.
- [30] M. Bedjidian *et al.*, Phys. Lett. **83B** (1979) 252.
- [31] G.P. Gopal et al., Nucl. Phys. **B119** (1977) 362.
- [32] T. Harada, Private communication (2006).
- [33] H. Noumi, private communication (2005).
- [34] K. Nakazawa et al., J-PARC proposal, “Systematic study of double strangeness system with an emulsion-counter hybrid method”.
- [35] K. Tanida et al., J-PARC proposal, “Measurement of X rays from  $\Xi^-$  atoms”.